EFFECT OF INITIAL OIL SATURATION ON IN-SITU COMBUSTION PERFORMANCE OF A CANADIAN BITUMEN

A Thesis

by

DENIS ALEKSANDROV

Submitted to the Office of Graduate Studies of
Texas A&M University
in partial fulfillment of the requirements for the degree of

MASTER OF SCIENCE

Chair of Committee,	Berna Hascakir
Committee Members,	Maria A. Barrufet
	Jerome J. Schubert
Head of Department,	A. Daniel Hill

August 2013

Major Subject: Petroleum Engineering

ABSTRACT

In-Situ Combustion (ISC) is a very complex thermal recovery process that is strongly affected by the chemical composition and physical properties of reservoir rock and fluids. Stability of the process depends on the amount of heat continuously generated from the chemical reactions between fuel formed during ISC and injected oxygen. Heat generation depends on the amount of fuel formed, which, in turn, is affected by initial oil saturation (IOS). Thus, in this study, ISC process dynamics were investigated at various saturations on 7.5 °API Peace River bitumen, under 3.4 l/min air injection rate.

Through one-dimensional combustion tube experiments higher combustion front temperatures were observed for increased IOS. The degree of bitumen upgrading was determined in terms of viscosity and API gravity changes. Correlations for hydrogen-carbon ratio, air requirement, consumed fuel, and combustion front velocity were obtained. Good burning characteristics of Peace River bitumen resulted in stable self-sustained combustion with 26.01% IOS. However, an experiment with 13.39% IOS failed because of insufficient fuel generation.

Furthermore, X-Ray cross-sectional images were taken along the combustion tube after each run to support and enhance the interpretation of experimental results. Particularly, fluctuations in concentrations of produced gas composition were explained with computed tomography (CT) data.

DEDICATION

To my Mother

ACKNOWLEDGEMENTS

I want to express the highest appreciation to my advisor, Professor Berna Hascakir. Without Dr. Hascakir's support and guidance this study couldn't be fulfilled. Her encouragement, faith in my abilities and her constant pressure not only extended my limits and allowed to succeed in research, but also developed a proper attitude towards work and education.

I would like to thank Professor Maria A. Barrufet, who gave me an opportunity to study in Texas A&M University. Being one of my committee members, she provided a lot of valuable remarks and advices, which highly improved my Thesis. It was an honor to work in Ramey Thermal Recovery Laboratory that Dr. Barrufet kindly provided for the whole research.

I would like also to acknowledge my committee member, Professor Jerome J. Schubert. His knowledge and experience helped a lot during the whole process of education and highly contributed to my excellent completion of drilling courses.

My thanks are also devoted to Darla-Jean Weatherford for thorough revision of this Thesis and teaching of a proper way to express my ideas clearly.

I am also thankful to Eleanor Schuler, who managed the documentation part of my education and ensured the meeting of all requirements and deadlines in Texas A&M University.

I also thank Daulat D. Mamora for equipping the Ramey Thermal Recovery Laboratory.

My deep gratitude is directed to Anatoly B. Zolotukhin, who not only made the joint program between Texas A&M University and Gubkin RSU of Oil&Gas real, but also assisted and supported me a lot during education process.

I want to thank my advisor in Gubkin RSU of Oil&Gas, Aleksey V. Dengaev, for the help provided during years in Gubkin University and for the desire to give me field-related knowledge through real case assignments.

Thanks are also extended to Dmitry N. Lambin, who secured the meeting of all requirements and managed the documentation part of my education in Gubkin RSU of Oil&Gas.

Finally, I express the deepest gratitude to my family and friends, whose infinite support and love help me to withstand all difficulties and problems that I face in life.

NOMENCLATURE

EOR	Enhanced Oil Recovery
SF	Steamflooding
ISC	In-Situ Combustion
SARA	Saturate, Aromatic, Resin, Asphaltene
IOS (S_{oi})	Initial Oil Saturation (%)
CT	Computed Tomography
STA	Simultaneous Thermal Analysis
HTO	High-Temperature Oxidation
LTO	Low-Temperature Oxidation
CHOPS	Cold Heavy Oil Production with Sand
$\emptyset$	Porosity, %
D_{CT}	Combustion Tube Inner Diameter, cm
L_{CT}	Combustion Tube Length, cm
V_{CT}	Combustion Tube Volume, cm^3
V_{pv}	Pore Volume for Sand Pack, cm^3
S_{wi}	Initial Water Saturation Value, %
O_2	Oxygen Mole Concentration, mol.%
CO_2	Carbon Dioxide Mole Concentration, mol.%
CO	Carbon Monoxide Mole Concentration, mol.%
N_2	Nitrogen Mole Concentration, mol.%

$[O_2]$	Normalized Oxygen Mole Concentration, mol.%
$[CO_2]$	Normalized Mole Carbon Dioxide Concentration, mol.%
$[CO]$	Normalized Mole Carbon Monoxide Concentration, mol.%
$[N_2]$	Normalized Mole Nitrogen Concentration, mol.%
$V_{i\text{-}lab}$	Injected Gas Volume, scf
$V_{burned\text{-}sand\text{-}lab}$	Burned Sand Volume, ft^3
H/C, n	Hydrogen-Carbon Ratio
m	CO to CO_2 molar Ratio
R	N_2 to O_2 Mole fraction in the feed gas (injected air)
Y	Oxygen Utilization, frac.
F	Fuel Molecular Mass, gr/mol
A_r	Air Requirement, scf/ft^3
C_f	Fuel Consumed per Volume of Sand Burned, lb/ft^3
$H_c\ (\Delta H)$	Heat of Combustion (Enthalpy), BTU/lbm
V_f	Combustion Front Velocity, cm/hr

TABLE OF CONTENTS

LIST OF FIGURES

Page

LIST OF TABLES

Page

CHAPTER I

INTRODUCTION AND LITERATURE REVIEW

Petroleum, being the dominant source of energy and the main raw material for petrochemical industry, has become the focus of increasing concern as "easy" reservoirs have become depleted. The ultimate recovery factor in the industry is as low as 35% (Labastie, 2011), which means that the majority of oil remains unrecovered. This situation compels the petroleum industry to redirect its attention towards unconventional resources, which to be profitable require technologies that may provide high recovery ratio with reasonable implementation costs.

A large portion of unconventional resource base is occupied by extra-heavy oil and sands with low API gravity and high viscosities (Paszkiewicz, 2012). Their development can be accomplished most successfully with thermal enhanced oil recovery (EOR). Steamflooding (SF) is one of the most common and well-established thermal EOR today with a process displacement efficiency of about 65%. However, the ever-increasing gap between energy demand and supply necessitates more efficient recovery methods. Therefore, this study is devoted to In-Situ Combustion (ISC), a thermal method with a displacement efficiency as high as 95%. Because of poor areal and vertical sweep efficiencies, actual recovery cannot reach that level but equals about 65%, a much higher value than the corresponding 39% of SF process (Sarathi, 1998). Moreover, if ISC is implemented with modern emerging technologies, such as monitoring of thermal fronts

(Sen and Vedanti, 2008) and smart well technology (Rojas, 2011), the recovery efficiency can be increased significantly.

The main principle of ISC includes the injection of air (or enriched air) into the reservoir, although different modifications exist (Islam et al., 1989). Oxidation reactions taking place result in heat and gas production (mainly, CO_2, CO, N_2 and light hydrocarbons), which in turn displace the oil (Bourdarot and Ghedan, 2011). The approach of the combustion zone can be judged by an increase in gas production and its oxygen content, followed by a sharp increase in bottomhole temperature, ranging from 100 to 200°F.

An advantage of ISC is the produced oil that is upgraded due to high energetic nature of the process (Castanier and Brigham, 2003; Xia and Greaves, 2001; Xu et al., 2000). Thus, after combustion tube experiments with Venezuelan heavy oil Hascakir et al. (2011b) demonstrated an improvement in terms of API gravity measurements and change in composition of oil, rock and water. The API gravity upgrading was also noted by Rahnema et al. (2012), when the corresponding value increased from 8.24 to 10.4°API for Athabasca oil sand.

A wide operating range of field conditions is another advantage of ISC. For instance, extreme heat losses reduce the effectiveness of steam injection in deep reservoirs. Therefore, to achieve feasible recovery of such reserves, ISC can be implemented.

However, ISC still requires a substantial amount of optimization and field tests to lower the risks of field application (Regtien, 2010). According to worldwide EOR

survey (Koottungal, 2008) the share of US petroleum production due to ISC started to increase after 2004 and reached 17,025 b/d — 8.5 times its value for 2004 and 1.3 times with the value for 2006. The number is still insignificant — around 3% of total US EOR production (643,111 b/d in 2008). Despite the fact that some field projects exhibit outstanding results (Turta et al., 2005), the operators are still unwilling to implement ISC due to its complexity. Moreover, problems related with upscaling of laboratory results and forecasting of the ISC field performance remain. However, ISC provides a wide research prospective to improve application and engineering.

The research over ISC is usually led through combustion tube experiments to model the ISC field performance and through Simultaneous Thermal Analysis (STA), which examines the reaction kinetics of combustion process. Thus, STA has been accomplished by Moore et al. (1999) and Ren et al. (2005) to understand the nature of the oxidation reactions, and combustion tube experiments have been carried out by Greaves et al. (2000), Onishi et al. (2006), Hascakir et al. (2011a).

Upscaling of laboratory experiments for any recovery method can be achieved via analytical or numerical methods. However, due to extreme grid sensitivity and high complexity of chemical reactions, ISC modeling for field scale hasn't been obtained successfully yet (Glatz, 2012).

Analytical modeling remains the basis for numerical simulation, although difficulties with calculation of ISC volumetric sweep efficiency and combustion front-velocity exist.

First, a heat-transfer model was applied for analytical modeling (Penberthy et al., 1968). Then, it was developed starting from Vogel and Krueger (1955) and Ramey (1958), generalized by Bailey and Larkin (1959) and Chu (1963), and further extended by Thomas (1963), and modified by Penberthy and Ramey (1965). An alternative steady-state model was also developed, which included both simple reaction kinetics and heat transfer issues (Agca and Yortsos, 1985). Further development of analytical modeling was led through the consideration of thermal cracking reactions (Millour et al., 1985) and their consolidation with oxidation kinetic studies (Belgrave et al., 1993).

Characterization of a stable combustion processes during combustion-test experiments can be achieved with a descriptive moving-frame analytical model, developed by Sibbald et al. (1991). Another analytical model was proposed by Rodriguez and Mamora (2005) after six oxygen-enriched combustion tube experiments. This provides an accurate calculation of combustion-zone temperature profiles.

Moreover, analytical approaches were used to define ISC design parameters for field applications (Alexander et al., 1962; Nelson and McNeil, 1961). These parameters can only be obtained by processing readily available experimental data. But before calculation of ISC engineering parameters a good field candidate for the process application should be defined either through combustion tube or kinetics experiments.

To aid reservoir selection a number of screening guides have been developed, among which the most cited is by Taber et al. (1997) with updates by Al-adasani and Bai (2010) (Table 1). Unfortunately, the use of these tables is not proper for all reservoirs with different rock and fluid types. This reveals the need for additional research to

reduce the complexity of ISC dynamics for heterogeneous reservoirs that are good candidates for ISC application. Thus, the influence of various parameters in the screening table is further reviewed below.

Table 1. Screening guide example for ISC
(Taber et al., 1997)

Parameters, units		Screening Guide
Reservoir Characteristics	Oil Saturation, % PV	> 50
	Formation Type	Sand or Sandstone with High Porosity
	Net Thickness, ft	> 10
	Porosity, %	Not Critical
	Average Permeability, mD	> 50
	Depth, ft	< 11.500
	Temperature, °F	> 100
Oil Properties	Gravity, API	> 10
	Viscosity, cp	< 5.000
	Composition	Some Asphaltic Components

While oil composition appears to be noncritical factor (Table 1), its effect on ISC performance has been investigated by many scientists (Akin et al., 2000; Freitag and Verkoczy, 2005). Because it is impractical to define each component of crude oil, some sub-categorizations are used to characterize crude oil composition. These include saturate, aromatic, resin and asphaltene (SARA) fractions. Saturates are the "ignitor" fraction in oil. Because of high reactivity at low temperatures, these affect the process stability ahead of the combustion front (Kok and Karacan, 1997). Fuel that is consumed

during combustion is created mainly by asphaltene and less by resin and aromatic fractions (Verkoczy, 1993).

Heat generation due to fuel-burning reactions should be enough to exceed the activation energy barrier that is responsible for the fuel forming reactions; otherwise the process won't be self-sustained (Islam et al., 1989).

Activation energies and reaction constants for pyrolysis and oxidation reactions taking place during ISC can be determined by the Arrhenius model (Murugan et al., 2009). Heat of combustion can be calculated with the composition of produced gases obtained from combustion tube experiments (Burger and Sahuquet, 1972; Sarathi, 1998). To artificially regulate the fuel formation and combustion reactions, various catalysts can be considered, such as metallic salts (Kok and Bagci, 2004).

Beside oil composition, reservoir characteristics and their heterogeneities greatly affect the process performance. The knowledge of the reservoir geology is vital for ISC design, successful operation, and analysis of the field application (Earlougher Jr. et al., 1970).

Concern with reservoir depth is mainly bounded not with the combustion process itself, but with economic considerations, which are positive statistically for the depths below 11,500 ft. Thin reservoirs favor better vertical sweep efficiency and more uniform oil displacement, as the large density differences between gas and oil causes the first one to bypass (override) the oil bank in thick reservoirs (Boberg, 1988). Although low thickness has also a negative aspect as it may result in problems with self-sustained combustion under high overburden heat losses, technically successful field applications

exist: projects at Glen Hummel, Gloriana and Trix-Tiz oilfields with 8.77-ft, 4.4-ft and 9.1-ft values of net pay thickness (Buchwald Jr. et al., 1973) and a Fry in-situ combustion project in Illinois (Earlougher Jr. et al., 1970) with less than 5-ft thickness.

Formation thickness may be an important issue for oils hardly capable of auto-ignition, as the well-bore area of thick formations (>50 ft) requires more heat to reach the corresponding temperature than the thin ones. In such cases artificial ignition techniques, such as heating of the injection well-bore zone or pumping of a reactive compound prior air injection, are suggested to eliminate undesired expenses.

The value of permeability doesn't highly affect the combustion process, but reservoir heterogeneities in terms of permeability barriers can affect the combustion application differently. Vertical permeability barriers can favor the process as they may divide a thick reservoir into smaller layers—thus resulting in more uniform combustion—and may prevent the loss of injected air into the overburden stratum. Horizontal permeability barriers can spoil the process as the reservoir continuity will be decreased. The location of the wells according to directional permeability can maximize the recovery.

Fractures may impair the performance of ISC field application as the injected air will tend to choose the path of least resistance and reduce the amount of oxygen available for the combustion front reactions. High porosity values are desirable as they correlate with the amount of hydrocarbons the formation possesses.

Even if the reservoir possesses a high permeability region with favoring initial oil saturation and good porosity, an important characteristic of the reservoir should be

continuity of individual sand layers within the producing formation. Thus, poor continuity explains the failure of ISC projects at such fields as Ojai, Placerita Canyon and White Wolf in the early 1960s (Sarathi, 1998).

Rock composition affects the amount of fuel available for combustion, thus, the presence of kaolinite and illite clays and rock minerals such as calcite, pyrite, and siderite favor fuel-forming reactions (Sarathi, 1998).

As was mentioned previously, the sustainability of the combustion process depends on the amount of heat continuously generated with the chemical reactions between fuel formed during ISC and injected oxygen. Furthermore, while the amount of fuel formed affects the heat generation, it is strongly influenced by initial oil saturation (IOS).

To investigate the sensitivity of heavy crude oil combustion towards initial oil saturations and other parameters including air flux and activation energies of a chosen reaction scheme an uncertainty analysis was conducted by Ogunbanwo et al. (2012) with 10 °API gravity oil. The study determined that the value of initial oil saturation strongly affects the fuel deposition and within the range of 45- to 70%, it results in successful ignition and propagation of the front as well as in optimal recovery factor.

Table 2 gives successful and failed ISC field projects. Underlined values given in Table 2 indicate parameters that are out of the screening range. The success or failure of those projects doesn't correspond to the screening guide given in Table 1. Thus, an example can be given with Little Tom oilfield that appeared to be a perfect candidate for ISC, but was aborted because of failure to ignite (Chu, 1982). May-Libby, Sloss and

Fosterton Northwest oilfields, which were all successful in terms of ISC application (Table 2), have IOS values below the recommended ones, but no problems were encountered with ignition or sustaining the combustion.

Table 2. Successful and failed ISC field projects
(Chu, 1982)

Parameters, units		Oilfields			
		Successful		Failed	
		May-Libby	Sloss	Fosterton Northwest	Little Tom
Reservoir Characteristics	Oil Saturation, % PV	42.8	30	45.2	60
	Formation Type	Sandstone	Sandstone	Sand	Sandstone
	Net Thickness, ft	8.3	14.3	27.7	14
	Porosity, %	31.2	19.3	28.8	22.3
	Average Permeability, mD	1,069	191	958	64
	Depth, ft	3,400	6,200	3,100	2800
	Temperature, °F	135	200	125	125
Oil Properties	Gravity at Reservoir Conditions, °API	40	38.8	23.6	18
	Viscosity at Reservoir Conditions, cp	3	0.8	13.5	90

Applicability of the ISC process for saturations less than 50% has also been proven in laboratory studies. Thus, Greaves et al. (2000) conducted combustion tube runs to simulate the ISC in post-waterflooded media and light reservoirs. The runs were

successful, and fuel laydown was sufficient to sustain the combustion, although the ISC with IOS values below 48% for heavy and 41% for light oils haven't been studied. Analogous experiments were carried out by Onishi et al. (2006), whose research included two combustion tube runs with light oil for the values of 16.4% and 22.3% initial oil saturations respectively. Both runs demonstrated a stable combustion front. Moreover, a self-sustained combustion was observed during combustion tube experiment with a 20% IOS zone of Venezuelan 8.65-°API gravity oil (Hascakir et al., 2011a). In addition, good burning characteristics of 8-°API Athabasca bitumen resulted in successful combustion process for 13.55% IOS (Xia and Greaves, 2002). Finally, self-sustained ISC was achieved during combustion tube experiments with 12.8-°API Brazilian heavy oil and 25% of both initial oil and water saturations (Chicuta and Trevisan, 2009)

ISC is a very complex and yet insufficiently studied process. Today the only sure way to check its' viability for the reservoir is to run a high-priced pilot test. To avoid these expenses and foresee possible problems a numerical simulation of ISC field performance should be achieved. In order to aid the development of numerical models, sensitivity studies with reservoir heterogeneities and initial oil saturations in particular were conducted experimentally on a Canadian bitumen in this study.

CHAPTER II

MATERIALS AND METHODS

Sample Characterization

The effect of initial oil saturation is tested on Peace River bitumen (Figure 1). Oil sand reservoir covers an area of approximately $6.2*10^6$ m^2 and contains nearly $12*10^{12}$ m^3 of bitumen (Hamm and Ong, 1995). The object of interest is Basal Transition Zone, which has a permeability of 1,650 md. Water saturation for that zone is greater than 30%. Thus, initial water saturation during the experiments was chosen as a constant value of 35%. The reservoir properties are summarized in Table 3.

Table 3. Peace River reservoir rock and fluid properties (Hamm and Ong, 1995)

Parameters, units		**Peace River Area**
Bitumen	Oil Gravity, °API	7.5
	Viscosity at 25 ^{0}C, cp	72600
	Molar Mass, g/mol	527.5
	Asphaltenes, wt.%	20.5
Reservoir	Pressure, psi	536.6
	Temperature, °C	16.7
	Bubble Point, psi	464.1
	Thickness, ft	85.3
	Depth, ft	1807.74
	Maximum Oil Saturation, %	84
	Porosity, %	28
	Vertical - Horizontal Permeability Ratio (K_v/K_h)	0.3
	Maximum Oil Saturation, %	84

Figure 1. Geographical location of Peace River area (Alberta Geological Survey, 2012)

Experimental Procedure

For the present research, an experimental setup (Figure 2) initially created by Penberthy and Ramey (1965) and modified by Rodriguez and Mamora (2005) was used.

A combustion tube is a stainless steel pipe with a 101.2-cm length, an outer diameter of 7.62 cm, and a wall thickness of 0.16 cm. Copper gaskets were used to seal the flanges at both ends. To prevent sand production, stainless steel screen was used at the production end. Temperature profiles are recorded at 14 different positions with J-

type thermocouples inserted in 1/8-in tubing (Table 4). The number of thermocouples, used for each experiment varies, as some were broken during combustion tube runs. Therefore, their measurements were excluded from temperature profiles.

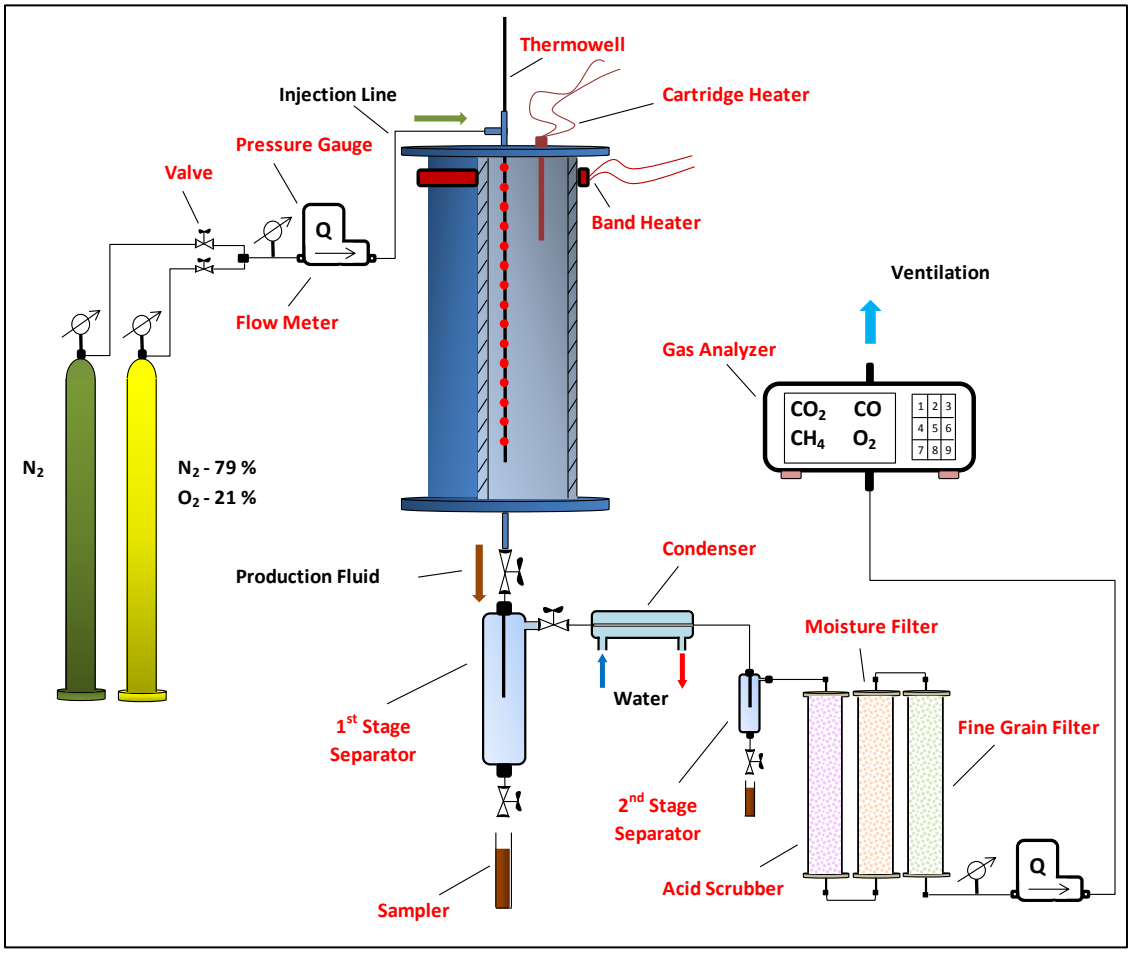

Figure 2. Experimental setup

Table 4. Thermocouple positions for all combustion tube experiments

Therm. #	Thermocouple Position, Measured from the Top of Combustion Tube, cm					
	Exp. I	**Exp. II**	**Exp. III**	**Exp. IV**	**Exp. V**	**Exp. VI**
1	-	-	-	11.75	-	11.75
2	14.92	14.92	14.92	-	14.92	14.92
3	26.04	26.04	26.04	26.04	-	-
4	30.32	30.16	30.16	30.32	30.32	30.32
5	-	33.18	33.18	33.18	-	-
6	36.83	36.83	36.83	36.83	36.83	36.83
7	45.40	-	-	-	45.40	-
8	-	-	51.28	-	51.28	-
9	59.37	59.06	59.06	59.37	59.69	59.37
10	-	-	-	-	64.61	-
11	73.50	73.66	73.66	73.50	73.50	73.50
12	-	78.58	78.58	-	-	-
13	-	-	-	-	83.98	-
14	96.36	-	-	96.36	96.36	96.36

Samples for combustion tube runs consisted of 20- to 40-mesh sand that corresponded to 32% porosity, kaolinite clay, water, and oil. First, 84 weight percent of sand was mixed with 15 weight percent of clay (Bayliss and Levinson, 1976). Then, fixed volume of water was added, which corresponded to 35 volume percent. Finally, oil was added at different initial oil saturations for each experiment. Table 5 summarizes initial fluid saturations that were used in each experiment. Rest of the pore volume was occupied by air. Detailed methodology of sample preparation step is listed in Appendix B. Other heterogeneities and inconsistencies, such as packing force, were minimized as much as possible.

Table 5. Initial fluid saturations for each experiment

Parameters, units	Experiments					
	I	II	III	IV	V	VI
Initial Water Saturation, %	32.88	34.96	34.05	34.03	35.63	34.45
Initial Oil Saturation, %	13.39	26.01	33.77	42.19	53.02	42.10
Initial Gas Saturation, %	53.73	39.03	32.18	23.78	11.35	23.45
Total, %	100	100	100	100	100	100

To eliminate heat losses, the combustion tube was wrapped with an insulator and placed into a vertical steel jacket with inner diameter 16.5 cm (6-1/2 in) and outer diameter of 20.32 cm (8 in).

Ignition was initiated with one cartridge (600 W) and two band heaters (400 W). After the temperature inside the combustion tube reached 500-520 °C, the nitrogen injection was changed to air injection and heaters were switched off. Composition of injected air included N_2 (79%) and O_2 (21%). Experiments were conducted at 100-psi back pressure and under 3.4-l/min air flow rate. Temperature profiles, inlet and outlet pressures, and gas flow rates with the produced gases compositions were continuously recorded by "LabVIEW" software. Produced oil was collected into 75-ml sample cylinders from the first stage separator. Light hydrocarbons and water vapor were condensed in the second stage separator, which was cooled by continuous water circulation.

Experiment VI was conducted to repeat the Experiment IV and to verify the accuracy of the experimental procedure by using same initial and experimental conditions.

Postmortem analysis of each experiment was visualized with a CT scanner to enhance the interpretation of experimental data. SIEMENS SOMATOM CT Scanner at Texas A&M Large Animal Hospital was used for this purpose. Cross-sectional images were acquired with 140 mAs and 120 kV tube current and voltage respectively. One-second rotational time and a three-millimeter distance between slices were set up for images.

CT scanning is a non-destructive imaging technology which provides information about the density change of the porous medium in Hounsfield units. A cross-sectional image that was further processed with Image-J software is given in Figure 3 as an example. White dots represent the position of thermowells in this figure. While lighter color represents denser medium, darker color corresponds to less dense medium. Therefore, in Figure 3, dark purple and almost black zones display void spaces created at combustion front due to highly energetic nature of high-temperature oxidation (HTO) reactions.

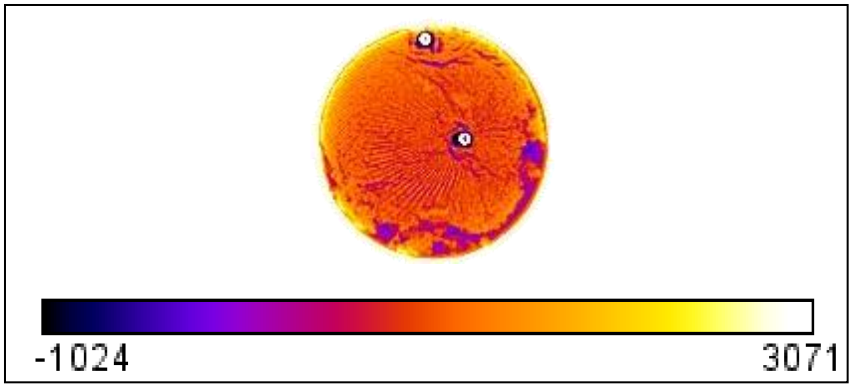

Figure 3. CT cross-sectional image example

Analytical Model

In this thesis, an analytical approach, which was constructed by Nelson and McNeil (1961) was combined with Benham and Poettman (1958) and Sarathi (1998) to analyze experimental results.

Mole percents of O_2, CO_2, CO and CH_4 in produced gas measured continuously during each experiment were used in analytical model Nitrogen in air was assumed inert so, not consumed during the experiments (Nelson and McNeil, 1961). There are some other gases produced during combustion, such as H_2S, NO_X, SO_X, etc. But the amount of these can be ignored beside other combustion gases. Therefore, N_2 is assumed in produced gases apart from O_2, CO_2, CO and CH_4 mole %:

$$N_2 = 100 - (O_2 + CO_2 + CO + CH_4)$$

Existing analytical methods are based on O_2, CO_2, CO and N_2 mole % (Table 6). Therefore, model calculations were started with the normalization of the produced gases. First, a stable zone was selected and the gas composition within the stable zone was

normalized. Then, the following formulas were utilized to calculate important ISC parameters analytically for different initial oil saturations. Sample calculation for Experiment II (26.01% IOS) is given in Appendix C.

Table 6. Laboratory data required for analytical analysis

Laboratory Data		
Parameters, units		**Symbol**
Composition of Injected Air, mol. %	Nitrogen	N_{2i}
	Oxygen	O_{2i}
Average Gas Composition of Produced Gases, mol.%	Oxygen	O_2
	Carbon Dioxide	CO_2
	Carbon Monoxide	CO
	Nitrogen	N_2
Injected Gas Volume, scf		$V_{i\text{-}lab}$
Burned Sand Volume, ft^3		$V_{burned\text{-}sand\text{-}lab}$

1. For the fuel burning reaction the following stoichiometry is defined (Benham and Poettman, 1958; Sarathi, 1998):

$$CH_n + \frac{1}{Y}\left(\frac{2m+1}{2m+2} + \frac{n}{4}\right) O_2 + \frac{R}{Y} \cdot \left(\frac{2m+1}{2m+2} + \frac{n}{4}\right) N_2$$

$$\rightarrow \frac{m}{m+1} CO_2 + \frac{1}{m+1} CO + \frac{1-Y}{Y}\left(\frac{2 \cdot m+1}{2 \cdot m+2} + \frac{n}{4}\right) O_2 + \frac{n}{2} H_2O$$

$$+ \frac{R}{Y}\left(\frac{2m+1}{2m+2} + \frac{n}{4}\right) N_2$$

$$n = \frac{H}{C} = \frac{4\left(\frac{[N_2]}{R} - [CO_2] - \frac{[CO]}{2} - [O_2]\right)}{([CO_2] + [CO])}$$

$$m = \frac{[CO]}{[CO_2]}$$

$$R = \left(\frac{N_{2i}}{O_{2i}}\right)_{feed\ gas}$$

where H/C is an atomic ratio that defines composition of formed fuel and $[N_2]$, $[CO_2]$, $[CO]$, $[O_2]$ are normalized values of produced gases

2. Oxygen utilization is the molar percentage of oxygen consumed in oxidation reactions, and it is calculated in fraction (Sarathi, 1998):

$$Y = \frac{\frac{[N_2]}{R} - [O_2]}{\frac{[N_2]}{R}}$$

3. Oxygen/Fuel ratio defines the minimum amount of oxygen needed to consume a unit mass of fuel, which is given in scf/lbm (Sarathi, 1998):

$$\frac{O_2}{Fuel} = \frac{379\frac{[N_2]}{R}}{F}$$

where F – fuel molecular mass that is defined with the following formula (Nelson and McNeil, 1961; Sarathi, 1998):

$$F = 12.011x + 1.008y$$

where:

$$x = [CO_2] + [CO]$$

$$y = 4\left(\frac{[N_2]}{R} - [CO_2] - \frac{[CO]}{2} - [O_2]\right)$$

4. Air/Fuel Ratio is the volume of air required to consume a unit mass of fuel, defines in scf/lbm (Sarathi, 1998):

$$\frac{Air}{Fuel} = (1 + R)\frac{O_2}{Fuel}$$

5. Unreacted O_2 and Produced CO_2 , CO, N_2, scf (Nelson and McNeil, 1961):

$$Unreacted\ O_2 = \frac{V_{i-lab}\ [O_2]}{[N_2]\ \left(1 + \frac{1}{R}\right)}$$

$$Produced\ CO_2 = \frac{V_{i-lab}\ [CO_2]}{[N_2]\ \left(1 + \frac{1}{R}\right)}$$

$$Produced\ CO = \frac{V_{i-lab}\ [CO]}{[N_2]\ \left(1 + \frac{1}{R}\right)}$$

$$Produced\ N_2 = \frac{V_{i-lab}}{\left(1 + \frac{1}{R}\right)}$$

6. Fuel consumed per volume of sand burned, lb/ft^3 (Nelson and McNeil, 1961):

$$C\ in\ fuel\ burned = \frac{12}{379}(Produced\ CO_2 + Produced\ CO)$$

$$H\ in\ fuel\ burned$$

$$= \frac{4}{379}\left(\frac{Produced\ N_2}{R} - Unreacted\ O_2 - Produced\ CO_2 - 0.5\ Produced\ CO\right)$$

$$Total\ weight\ of\ Consumed\ Fuel = C\ in\ fuel\ burned + H\ in\ fuel\ burned$$

$$Fuel\ Consumed\ per\ Volume\ of\ Sand\ Burned = C_f$$

$$= \frac{Total\ Weight\ of\ Consumed\ Fuel, lb}{Burned\ Sand\ Volume, ft^3}$$

7. Air Requirement is the most important parameter for an operating company which reflects the expenses of ISC field application and characterizes the amount of air that should injected to sweep one cubic foot of sand pack, scf/ft^3 (Nelson and McNeil, 1961):

$$A_r = 379.1 \frac{X\, C_f}{\frac{O_{2i\, feed\ gas}}{100}\, K \left(12 + \frac{H}{C} ratio\right)}$$

where:

$$X = \frac{2\, Produced\ CO_2 + Produced\ CO}{2\, Produced\ CO_2 + 2\, Produced\ CO} + \frac{\frac{H}{C} ratio}{4}$$

$$K = \frac{(100 - 4.761\, Produced\ O_2)}{\left(100 + \frac{Produced\ O_2}{X} - Produced\ O_2\right)}$$

8. Heat of Combustion, BTU/lbm

The combustion-front movement depends on fuel formation which is controlled by the kinetics of the combustion process (Burger and Sahuquet, 1972). However, plenty of reactions take place during combustion. Burger and Sahuquet (1972) achieved a formula to calculate the heat of combustion by considering the bond energy between one carbon and oxygen atom:

$$H_c = \Delta H = \left[\frac{\left(478260 + 356130\, \frac{[CO]}{[CO_2]}\right)}{\left(1 + \frac{[CO]}{[CO_2]}\right)\left(12 + \frac{H}{C} ratio\right)}\right] + \left[\frac{\left(56115\ \frac{H}{C} ratio - 309060\right)}{\left(12 + \frac{H}{C} ratio\right)}\right]$$

CHAPTER III

EXPERIMENTAL RESULTS AND DISCUSSION

To reach the research objective of this study, five combustion tube experiments were conducted. Experimental parameters and conditions were kept constant during all runs; except for the initial oil saturation values that were varied between 13.39% and 53.02% IOS with a 10% increment in each experiment. Repeatability study was conducted with Experiment VI in which 42.1% IOS was used.

Effect of initial oil saturation are discussed with temperature profiles, produced gas compositions, postmortem pictures, CT cross-sectional images, oil recoveries, in-situ upgrading and ISC parameters calculated analytically. Experiment VI is not included to the discussion of the effect of initial oil saturation on ISC performance although, experimental data is provided.

Temperature Profiles

The primary data acquired from combustion tube experiments were the temperature profiles (Figure 4). Each line on Figure 4 represents the temperature at a fixed thermocouple position, measured from the top flange of the combustion tube. Zero time corresponds to the start of air injection.

During heating period under nitrogen injection pyrolysis reactions take place (Abu-Khamsin et al., 1988):

$$Heavy\ Oil \xrightarrow{Heat} Hydrocarbon\ Derivatives + Gas$$

These are endothermic reactions that produce a solid residue with a low H/C ratio. This residue is referred in literature as fuel or coke. Start of air injection results in exothermic fuel-burning reactions. Thus, a temperature jump for the very first thermocouple is observed in each experiment (Figure 4). The released heat is consumed ahead of the combustion front to generate fuel continuously. Fully oxygenated fuel creations take some time to stabilize the combustion process. This time is known as a transition period (Hascakir et al., 2011a) Therefore, transition period, which is characterized by different amounts of heat released during fuel-burning reactions, can be noticed for the first minutes of each experiment in Figure 4. If the process maintains continuous heat and fuel generation, the stable self-sustained combustion is observed after the transition period.

Temperature profiles show that successful combustion front propagation was achieved for Experiments II through VI. Insufficient amount of fuel generation during Experiment I (13.39% IOS) resulted in failure of self-sustained combustion process. Similar fading temperature trend was observed by Chicuta and Trevisan (2009) for 25% IOS of Brazilian heavy oil (12.8 °API).

Although the ISC process is self-sustained for all successful experiments, the performance differs. For instance, Experiments II and III don't exhibit as high and sudden temperature peaks above 800°C as experiments IV and V did.

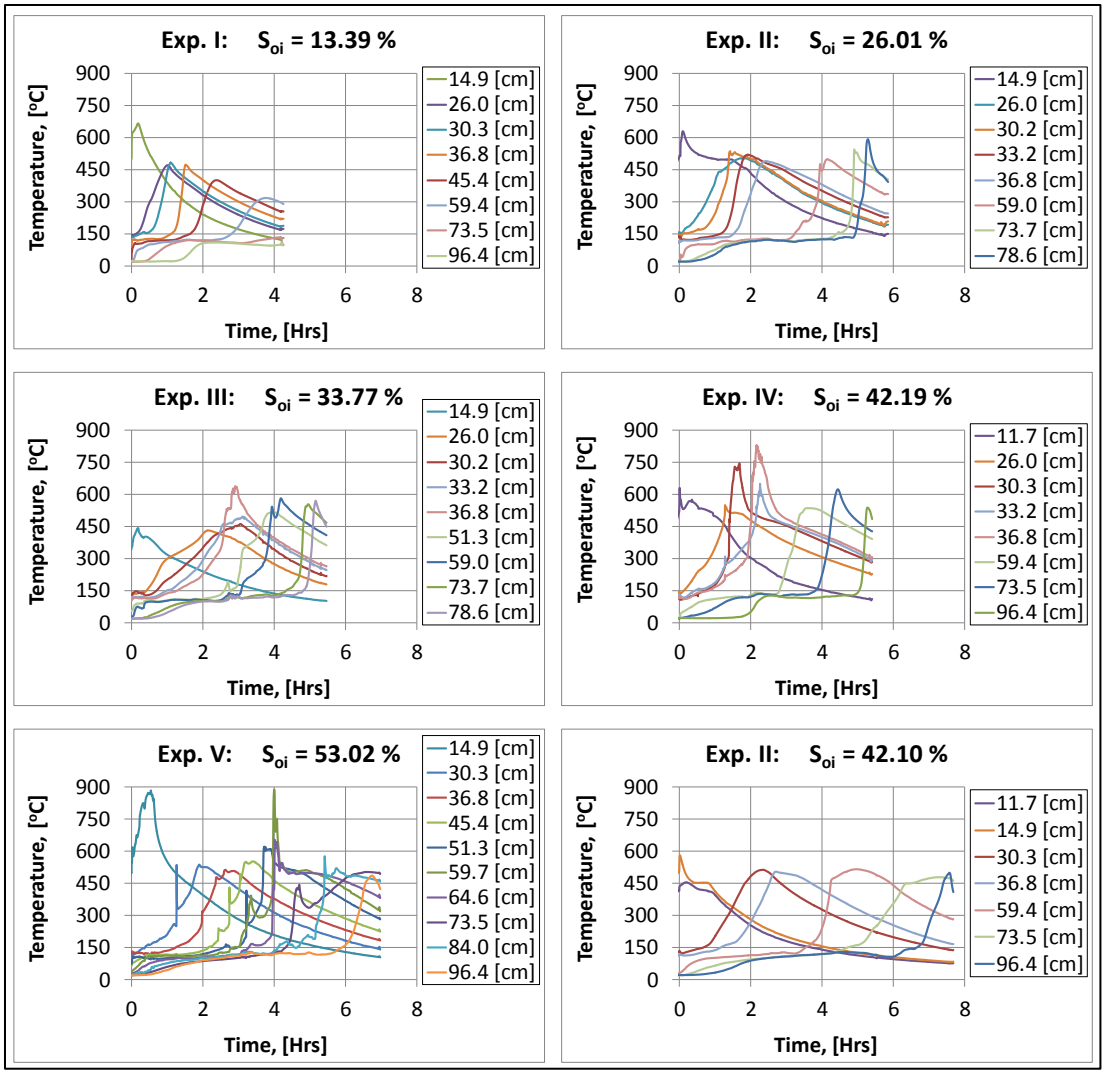

Figure 4. Temperature profiles for all experiments at different oil saturations

The heating period under nitrogen conditions is displayed on Figure 5. The voltage sent to band (400 W) and cartridge (600 W) heaters was increased manually through a voltage controlling device. This resulted in different heating rates, observed at Figure 5. Experiment III was the only one that included a cartridge heater in heating

configuration, and the slope downwards during the pyrolysis period reflects the time when this cartridge heater was broken.

When air injection starts, fuel that is formed under nitrogen condition ignites and results in a sharp temperature rise at the top of combustion tube (Figure 5). Experiment III had almost the same value of temperature increase as Experiments I, IV, and V. It is important to remember that the graph of Experiment III reflects the heat generated only by the oxidation reactions, but others reflect additional heat, received from heaters. During Experiment V heaters were turned off later than during the rest of the experiments, which resulted in a higher temperature at the top of combustion tube. Therefore, the temperature peak for Experiment V is not considered in the Figure 5.

The successful ignition and self-sustained combustion process in Experiment III revealed that Peace River bitumen possesses good burning characteristics. Air injection can be started at much lower temperature than 500-520 °C; however, for the purpose of consistency the target temperature to start air injection was kept constant during experiments.

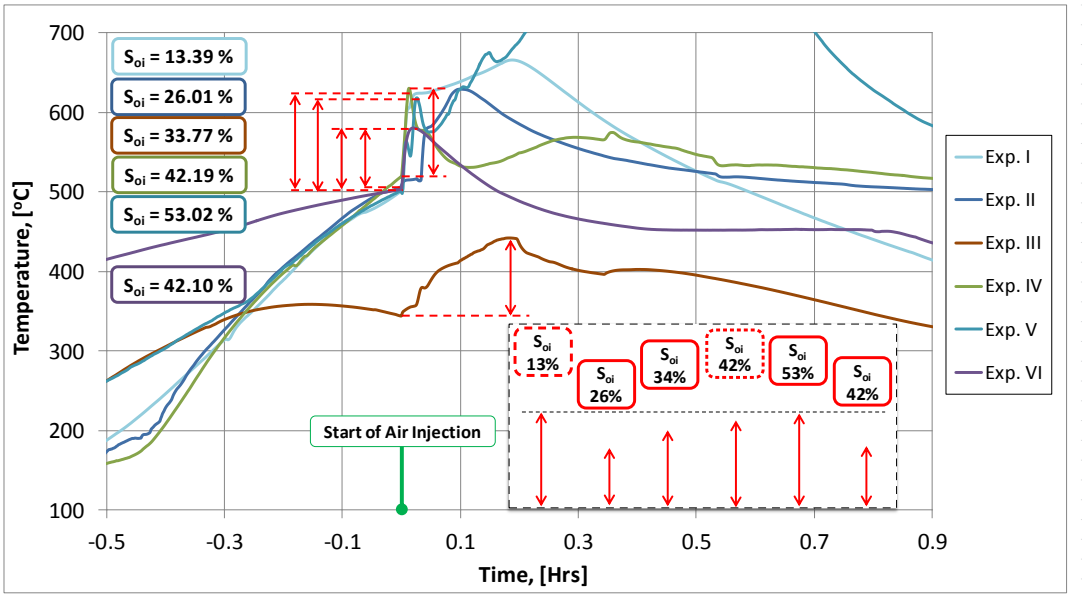

Figure 5. Temperature profiles for thermocouples at heater position for all experiments

Gas Compositions

To address the stable zone of the combustion process, the gas composition of the produced gases must be analyzed beforehand.

Successful combustion experiments are usually defined through gas composition graphs by the excess value of CO_2 concentration over the corresponding value for O_2. Thus, after air injection starts transition period, which varies with varying IOS, can be highlighted (Figure 6). Zero time in Figure 6 represents the start of air injection and transition period.

The conclusions drawn through temperature profiles can also be supported with gas composition graphs, which show the success of Experiments II through VI (Figure 6). The concentration of O_2 is dominant during Experiment I; low amount of

CO_2 is produced. Since oxygen is not effectively consumed for Experiment I, unsuccessful combustion front propagation for 13.39 % IOS case is observed.

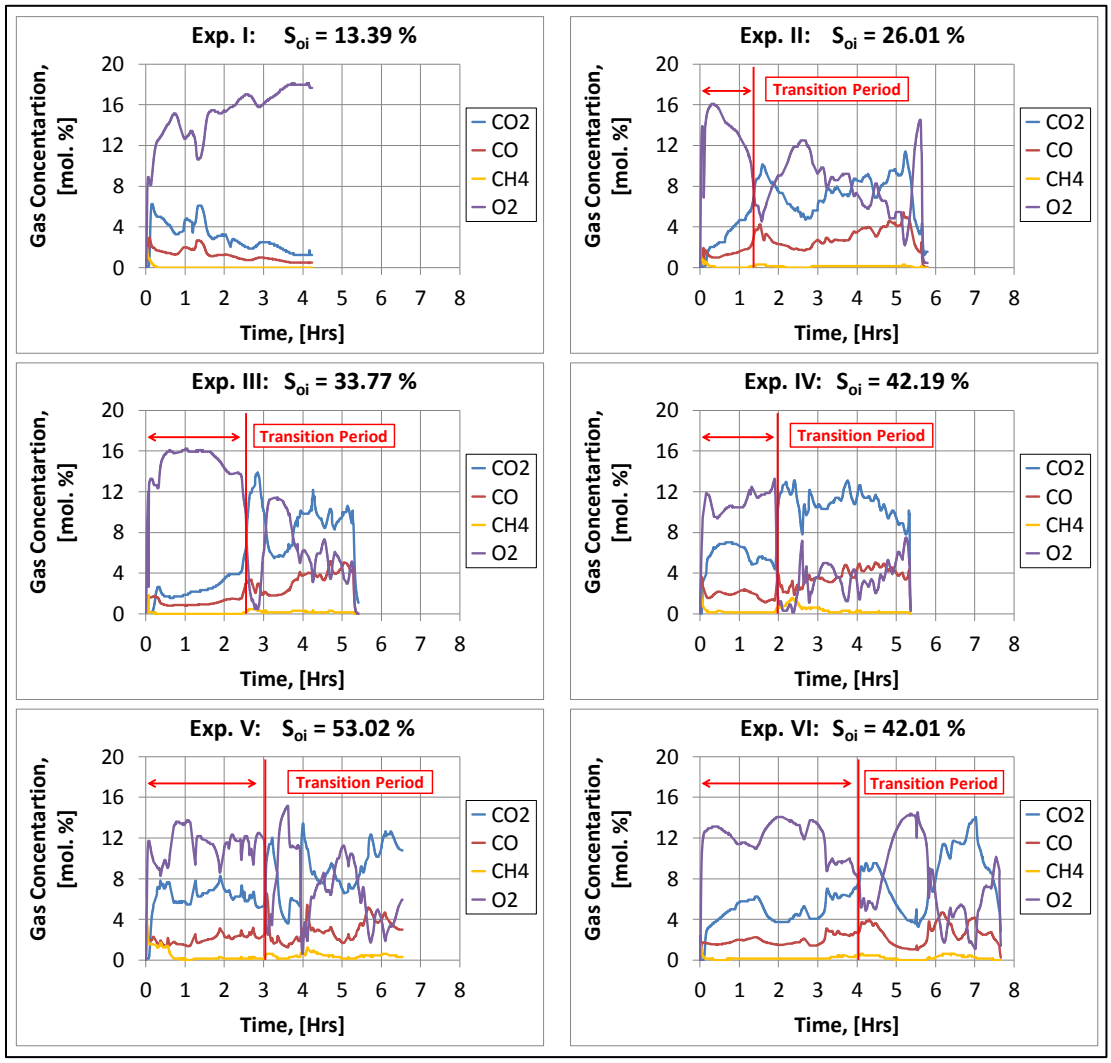

Figure 6. Gas compositions with determined transition periods for all experiments at different oil saturations

Stable period is defined primarily by considering the time, when CO_2 concentration starts to raise sharply and consequently exceeds the decreasing

concentration of O_2 (Figure 6). The beginning of stable period indicates the end of transition period.

The temperature profiles for stable period at 73.5 cm from air injection point are highlighted with Figure 7 and divided into three regions. Region 1 is the zone, where evaporation and visbreaking reactions, steam plateau, water and oil banks are observed. Region 2 includes cracking and combustion zones, and Region 3 defines the burned zone.

Heating periods, temperature values by the end of heating period, temperature jump just after the start of air injection, total experiment time as well as maximum reached combustion temperatures and heating rates for each experiment are summarized in Table 7.

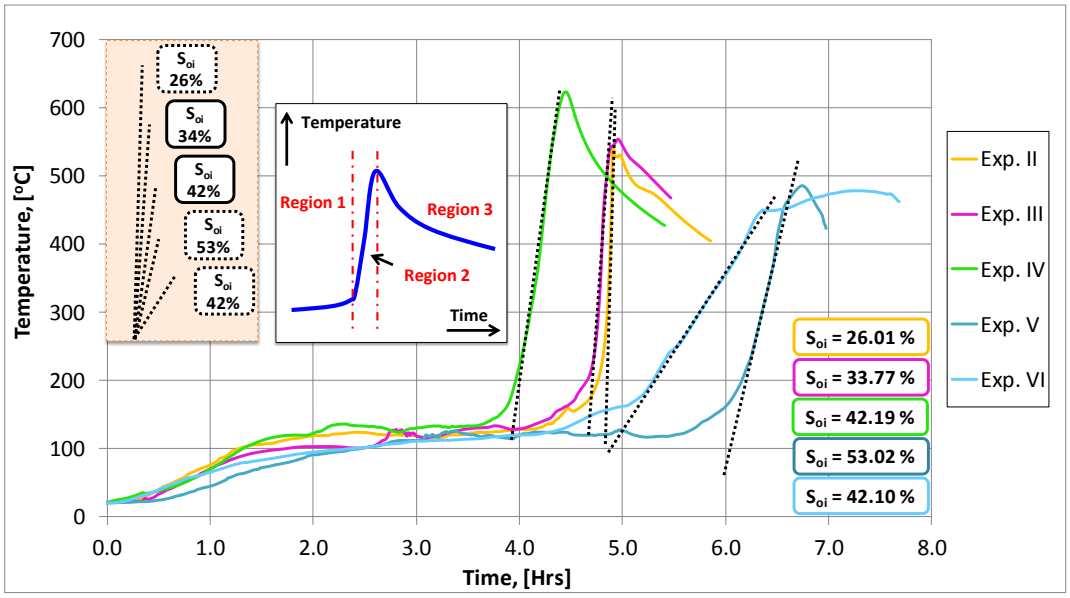

Figure 7. Comparison of temperature profiles for all experiments at a fixed position of thermocouple during stable combustion period.

Table 7. Evaluation of heating and stable periods

Parameters, units		Experiment Number					
		I	II	III	IV	V	VI
Initial Oil Saturation, %		13.39	26.01	33.77	42.19	53.02	42.10
Heating Time (N_2 Injection), min		45.1	55.7	93.3	59.7	68.0	105.2
Heating Start Temperature, °C		22.3	21.1	20.9	22.3	22.4	20.8
Heating End Temperature, °C		501.2	508.2	344.2	518.8	501.2	503.4
Jump of Temperature after the Start of Air Injection, °C		123.3	71.6	97.95	111.4	117.1	77.01
Experiment Time, min		258	348	327	324	415	456
Maximum Combustion Temperature, °C		483.2	592.3	638.5	829.3	887.6	515.4
Stabilization Time, min		-	82.55	154	116.9	183	243.3
Heating Rate at Stable Combustion, °C/min	Region 1	0.092	0.104	0.208	0.130	0.237	0.222
	Region 2	-	40.05	36.83	16.87	11.90	3.96

Postmortems

Postmortem pictures for all experiments are presented in Figure 8. In Experiments I and II, eight different zones were observed in postmortem pictures. Seven zones were noted for Experiment III and six zones for the rest of experiments. These zones were defined with visual inspection of color changes on postmortems of experiments. Each zone was named differently and given names are presented in Table 8.

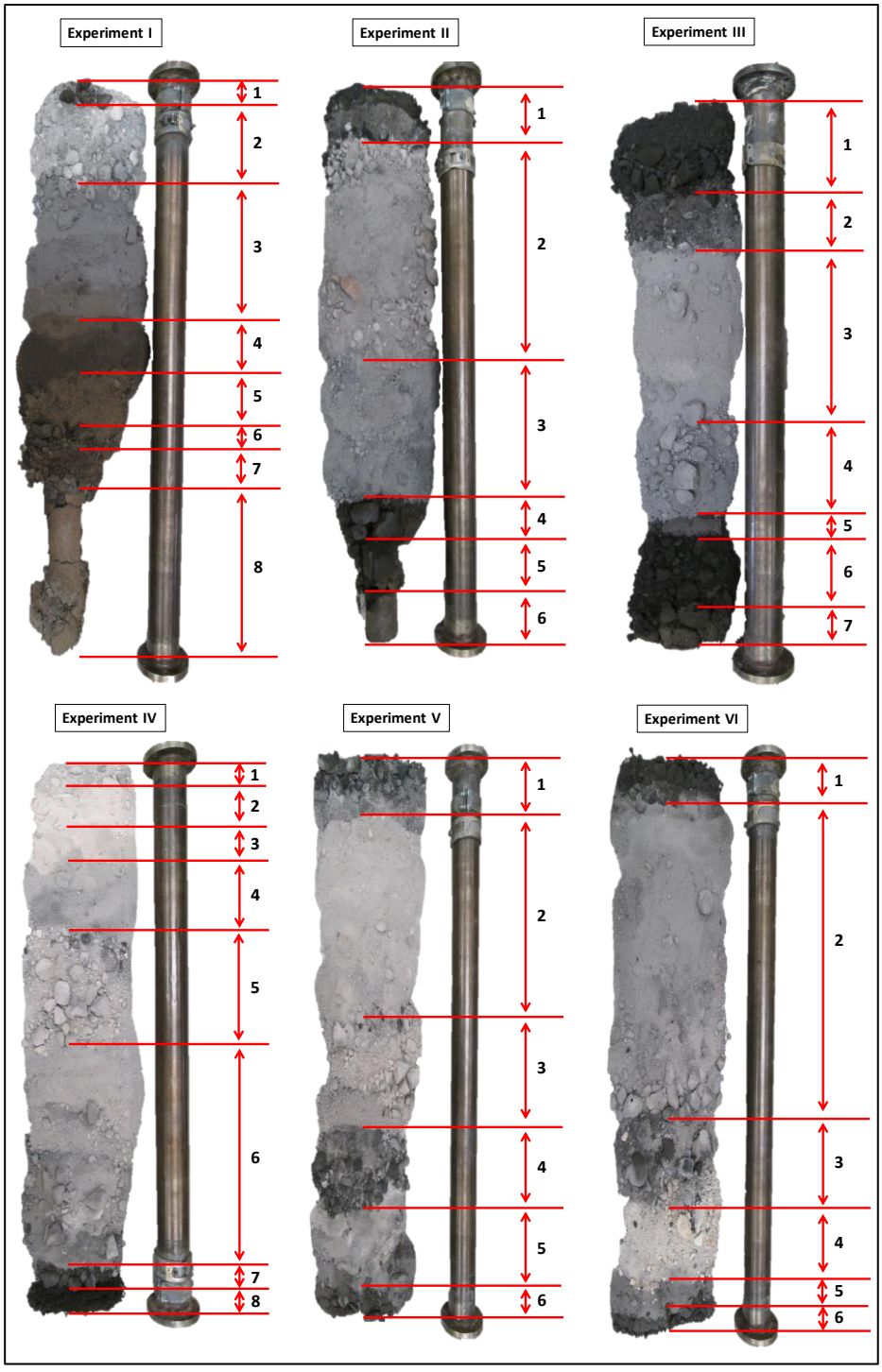

Figure 8. Overview of postmortems with highlighted zones for all experiments

Table 8. Postmortem zone classification for each experiment

Titles of Postmortem Zones	Numbers of Postmortem Zones					
	Exp. I	Exp. II	Exp. III	Exp. IV	Exp. V	Exp. VI
Fuel Formed During Heating Period	1	1	1	-	1	1
Transition Zone*			2	-		
Burned Zone	2-3	2-3	3-4	1-6	2-5	2-5
Transition Zone**	4-7		5			
Fuel Formed During Stable Combustion		4	6	7	6	6
Transition Zone***		5		8	-	-
Untouched Zone	8	6	7	-		

*Transition zone between fuel formed during heating period and burned zone

**Transition zone between burned zone and fuel formed during stable combustion

***Transition zone between fuel formed during stable combustion and untouched zone

Addition of clay to the sand pack enhanced the generation of fuel although, formed amounts weren't fully consumed during the combustion process. This was revealed by the grey color of burned zones and was supported by observations made during postmortem analysis. Thus, lumps of sand particles cemented with clay particles and combustion residues were observed. Consolidation most likely was caused by highly energetic nature of high-temperature oxidation reactions, which formed flow channels by moving and compressing the sand particles.

The comparison of temperature profiles (Figure 4) and postmortem pictures (Figure 8) reveals that the color of the burned zone is lighter and average combustion

temperatures are higher for Experiments IV and V than for the rest of experiments. This means, that if high temperatures are observed, more fuel is consumed and less is left behind the combustion front.

Moreover, no coke zone was observed during Experiment IV at the top of the tube (Figure 8), where temperature reached the value of 883 °C (Figure 4). This indicates that the fuel formed during heating period under nitrogen injection can be totally consumed at around 900 °C.

Postmortems of Experiments V and VI contain regions (Zone 4 and Zone 3 accordingly), where most of fuel was not consumed. This should be addressed to the combustion front breakthrough, which can be traced through temperature profiles (Figure 4). Hence, temperature measurements of the thermocouple at 64.6 cm below from injection point exhibited a slow increase (at 5 hrs.) during Experiment V and later became equal to the values of the thermocouple at 96.4 cm position. This slow temperature rise happened because of the bypassed fuel that continued to react slowly with injected air. Poor sweep efficiency of injected air limited the full consumption of formed fuel. Same explanations are valid for Experiment VI.

Lengths and masses of each zone numbered in postmortem pictures (Figure 8) are listed in Table 9 and Table 10. Lengths were calculated with a measuring tape; therefore, experimental error of ±2 centimeters is expected. Masses were measured with a weighting machine, although mass losses of not more than 15 grams during postmortem analysis are assumed.

Table 9. Length comparison for postmortem zones

Zone #	Length of Postmortem Zone, cm					
	Exp. I	Exp. II	Exp. III	Exp. IV	Exp. V	Exp. VI
1	1.0	9.0	14.0	2.5	11.5	4.5
2	15.5	45.0	10.0	7.5	36.0	60.0
3	26.5	24.5	34.0	5.0	22.5	14.5
4	11.0	6.0	21.0	14.5	15.0	14.0
5	9.0	7.0	1.0	22.0	12.5	6.0
6	2.0	10.5	12.0	42.0	4.5	3.0
7	8.0	-	10.0	3.5	-	-
8	29.0		-	5.0		
Total	102	102	102	102	102	102

Table 10. Mass comparison for postmortem zones

Zone #	Mass of Postmortem Zone, gr					
	Exp. I	Exp. II	Exp. III	Exp. IV	Exp. V	Exp. VI
1	73.1	537.1	1231.0	193.9	803.0	314.7
2	1093.9	3364.5	890.1	468.0	2598.0	4099.8
3	1605.0	1611.4	1685.4	466.4	1659.0	1032.2
4	1017.2	364.2	1460.0	885.6	946.0	1055.7
5	500.4	536.5	83.1	1485.3	954.0	428.0
6	120.7	802.1	802.3	3061.7	351.0	191.1
7	335.2	-	961.0	163.7	-	-
8	2315.3		-	272.7		
Total	7060.8	7215.8	7112.9	6997.3	7311.0	7121.5

Analytical Model

As was mentioned previously, Nelson and McNeil (1961) model was combined with other studies (Benham and Poettman, 1958; Sarathi, 1998) to analyze the results of

6 combustion tube experiments. These analytical models start with the selection of stabilized period. Due to fluctuations within stable period in gas composition graphs (Figure 6) only representative zones were chosen and the average concentration values of each gas were defined (Table 11) Time periods of these zones reflect the time needed for combustion front to sweep 10 cm of sand pack during each experiment. Therefore, the same time periods were chosen to calculate combustion front velocities (Table 12).

Table 11. Average gas composition of produced gases for selected stable combustion zone (10cm)

Exp. #	Time Period of Selected Stable Combustion Zone, hrs	Average Gas Composition of Produced Gases, mol.%			
		CO_2	CO	CH_4	O_2
II	4.67 - 5.28	9.40	4.41	0.17	4.89
III	4.25 - 4.77	9.69	3.99	0.19	5.39
IV	3.66 - 4.28	11.94	4.23	0.22	2.68
V	5.60 - 6.43	11.60	3.98	0.47	3.43
VI	6.45 - 7.03	12.27	2.98	0.41	3.79

Table 12. Combustion front velocities for selected stable combustion zones (10 cm)

Exp. #	Time Period of Selected Stable Combustion Zone, hrs	Combustion Front Velocity	
		cm/hr	ft/day
II	4.67 - 5.28	16.39	12.91
III	4.25 - 4.77	19.23	15.14
IV	3.66 - 4.28	16.13	12.70
V	5.60 - 6.43	12.05	9.49
VI	6.45 - 7.03	17.24	13.58

The maximum temperature value observed at a fixed position represents the location of the combustion front at the measured time. Figure 9 shows the combustion front location in time and is used to determine its speed. Nonlinear lines show inconsistent combustion front velocities and breakthroughs along the tube. This should be attributed not only to stabilization of the combustion front, but also to heterogeneities in sand pack distribution. An ideal representation of uniform process-propagation behavior during stable combustion can be seen in the work of Sibbald et al. (1991), where original consolidated Athabasca oil sand core was used.

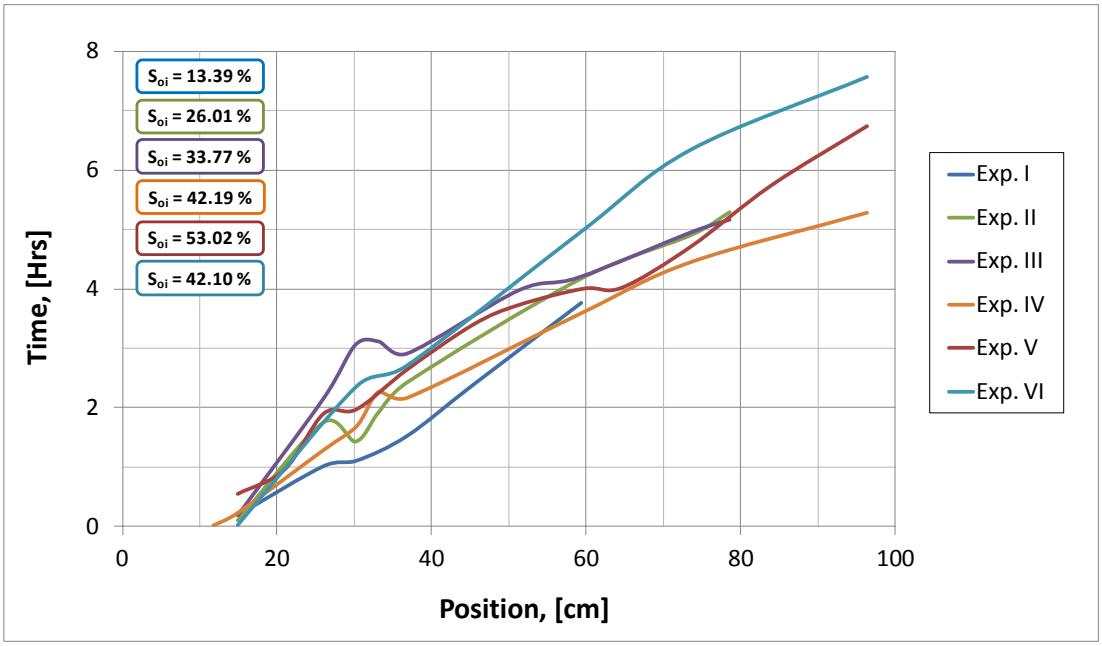

Figure 9. Combustion front position at different periods of time for all experiments

The relationship between combustion front velocities and IOS values shows a parabolic dependency (Figure 10). On one hand, while the amount of injected air remains constant (3.4 l/min), more fuel is deposited with the increased value of IOS. Therefore, increased air requirements for combustion front propagation result in slower combustion front velocities. Moreover, combustion front acts like a "bulldozer", which pushes the oil ahead of it (Gutierrez et al., 2009). Thus, increased loads due to IOS reflect in reduced combustion front velocity. On the other hand, insufficient amounts of fuel laid down for low IOS values cause reduced speeds as well (Armento and Miller, 1977). The maximum front velocity was achieved during Experiment III.

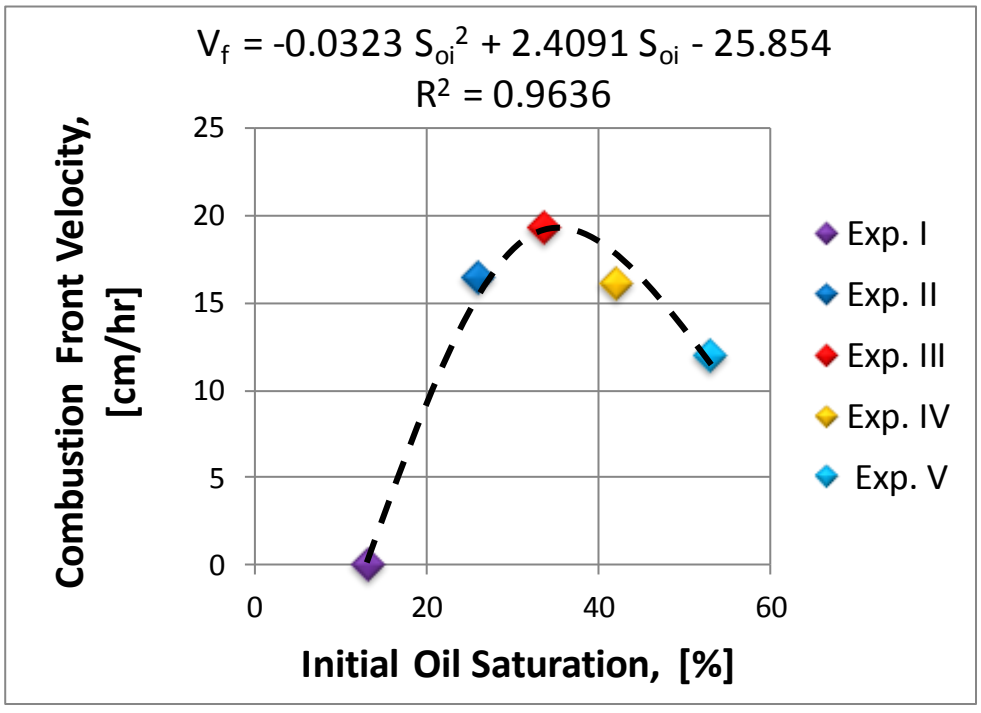

Figure 10. Comparison of combustion front velocities

Combustion tube experiments noted in literature and conducted for pressures between 80 and 600 psig revealed that the influence of pressure for the rate of combustion front propagation is small and can be neglected (Martin et al. (1957). Thus, combustion front velocities obtained during experiments under 100 psi pressure can be used for field-scale modeling of Peace River reservoir, which has 536.6 psi reservoir pressure.

As was mentioned previously, analytical analysis should be applied for stable combustion processes; otherwise, it will produce unreliable results. Because no stable zone was observed for Experiment I, it was excluded from analytical calculations. Defined average gas compositions and front velocities were used in analytical modeling to define operational parameters required for ISC field-scale application.

Figure 11 shows calculated ISC parameters, which exhibit several dependencies. The hydrogen-/carbon ratio decreases with the increase in IOS, the highest oxygen utilization is attributed to 42.19% oil saturation (Experiment IV), minimum fuel consumption is achieved during Experiment III, which also yielded the minimum air requirement. The reason, why Experiment II with 26.01% IOS doesn't fit the trends constructed in Figure 11, will be mentioned in the later sections.

The behavior of Peace River bitumen supports the statement of Abu-Khamsin et al. (1988) that the fuel H/C ratio decreases with increasing combustion temperatures. The minimum H/C ratio was obtained for Experiment V, during which the maximum combustion temperature was observed (Figure 4).

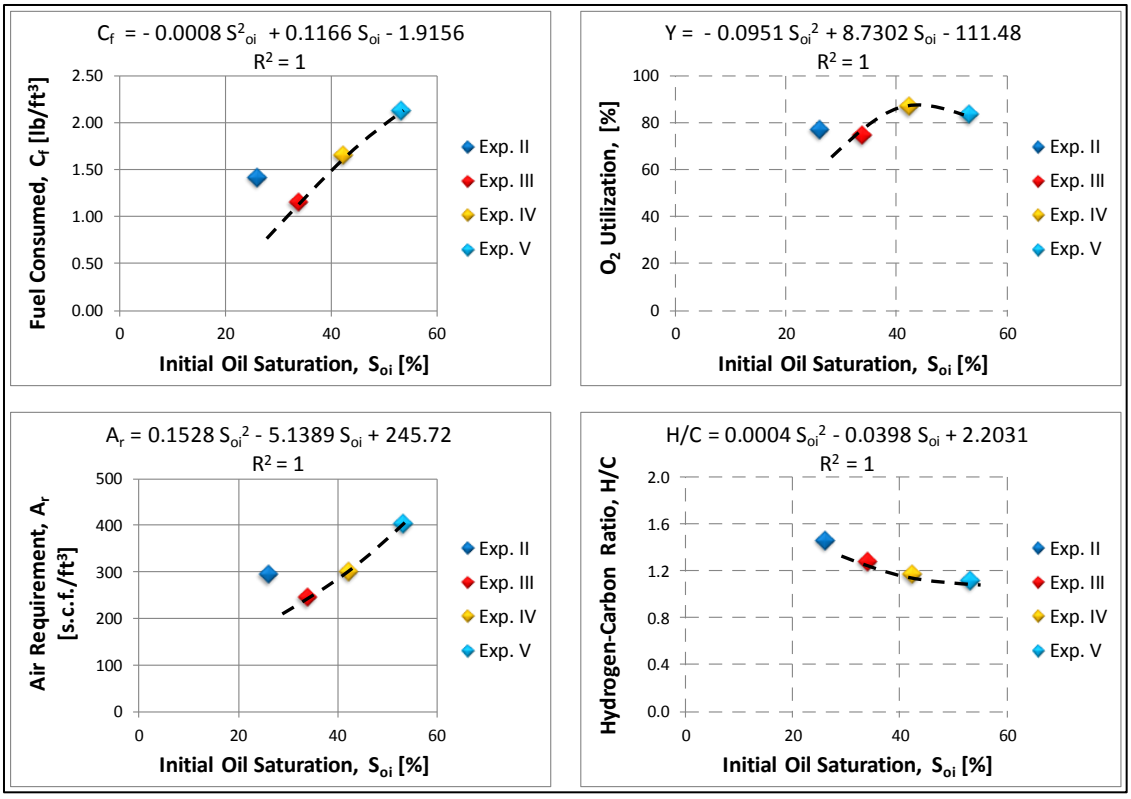

Figure 11. Comparison of analytical parameters

Moreover, the amount of fuel consumed during different initial oil saturations of Peace River bitumen exhibits behavior similar to 21.8-°API oil in Ottawa sand (Alexander et al., 1962). The relationship between fuel consumed and air requirement (Figure 12) is in agreement with the work of Alexander et al. (1962).

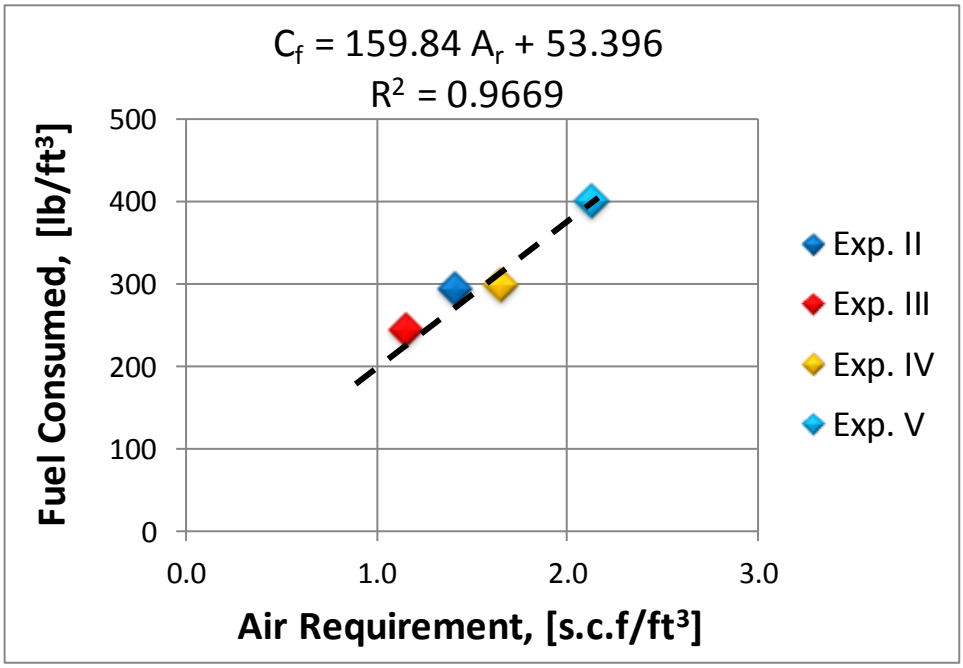

Figure 12. Fuel consumed versus air requirement

Oxygen utilization values commonly noted in literature are around 97% and even reach 100% for some field projects (Brigham et al., 1980). Those values are much higher than the oxygen utilization achieved during this study (Figure 11), which probably means that the fuel-burning reactions listed below reflect incomplete combustion:

- Experiment II:

$$CH_{1.46} + 1.327\ O_2 \rightarrow 0.32\ CO_2 + 0.68\ CO + 0.301\ O_2 + 0.732\ H_2O$$

- Experiment III:

$$CH_{1.27} + 1.289\ O_2 \rightarrow 0.292\ CO_2 + 0.708\ CO + 0.324\ O_2 + 0.638\ H_2O$$

- Experiment IV:

$$CH_{1.17} + 1.056\ O_2 \rightarrow 0.262\ CO_2 + 0.738\ CO + 0.132\ O_2 + 0.587\ H_2O$$

- Experiment V:

$$CH_{1.12} + 1.081\ O_2 \rightarrow 0.256\ CO_2 + 0.744\ CO + 0.173\ O_2 + 0.56\ H_2O$$

Mole difference between O_2 in reactants and products of listed above reactions gives the amount of oxygen that is consumed to burn one mole of formed fuel. Fuel-burning reactions indicate that this amount decreases with increasing IOS and therefore, decreasing H/C ratio.

Energy which is released during fuel burning reactions is characterized by the heat of combustion that is an intensive property and depends on the composition of fuel (H/C ratio), which varies among experiments. Analytically calculated values of heat of combustion show a slight decrease with decreasing H/C ratio and equal 15600 ±200 BTU/lbm. Self-sustained propagation of the combustion front indicates that the energy released during fuel burning reaction exceeds the activation energy of fuel forming reaction. This shows that Peace River bitumen favors the application of ISC.

Oil Recovery

Cumulative oil and water production is given in Figure 13. The amount of produced water corresponds to the amount packed, except for the Experiment I, which was terminated early since the combustion front was not propagating. Because of the same reason no oil production was observed for Experiment I. Only for Experiment III, oil production started just after water production ended. However, during Experiment V oil and water production started almost simultaneously.

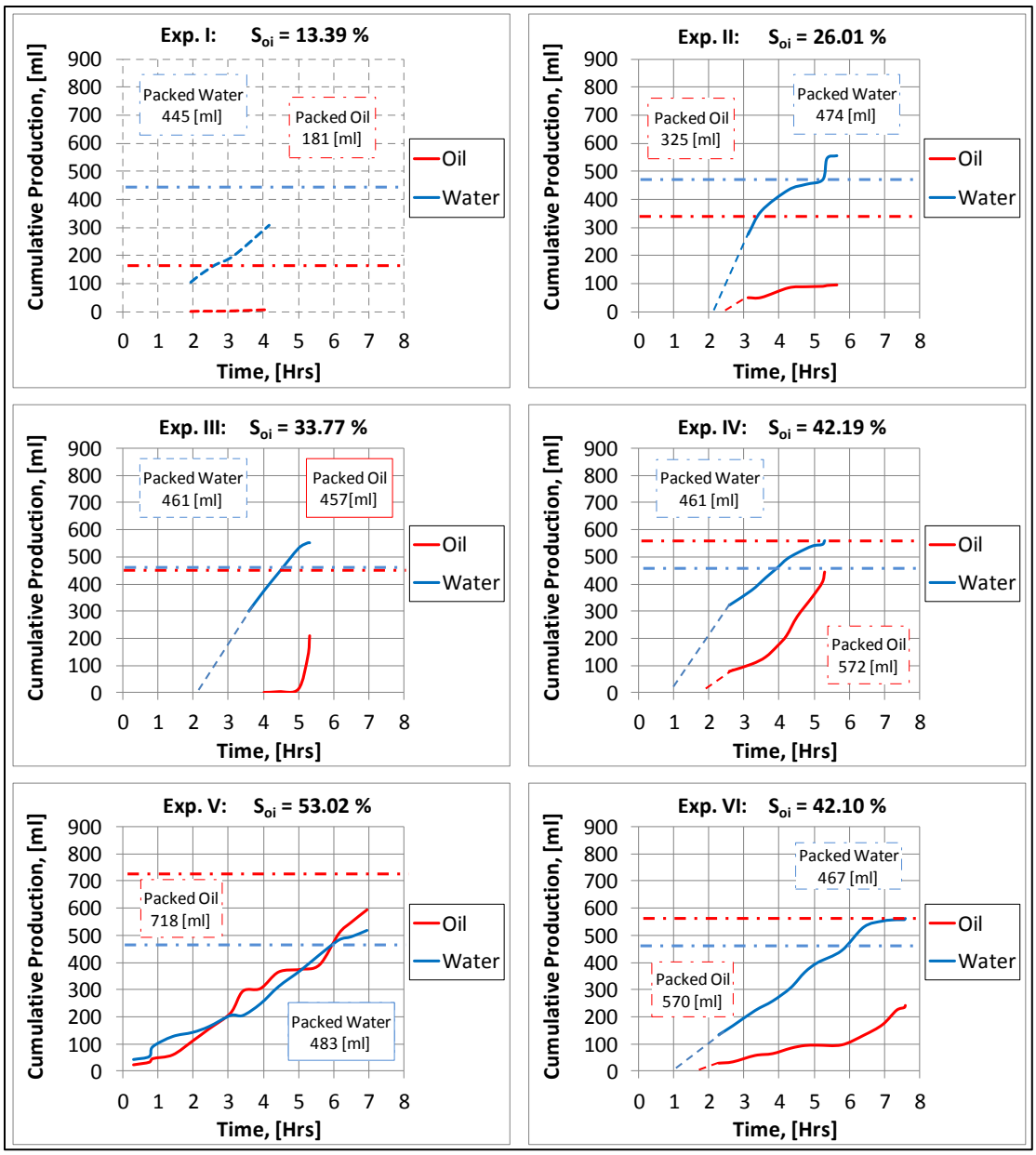

Figure 13. Cumulative oil and water production for all experiments

The early oil production for all experiments can be attributed to the oil breakthrough, which, possibly resulted because of the inserted thermocouples that

created an easy pathway for upgraded oil through the sand pack. An example of such behavior can be seen on Figure 14, which represents the bottom of the combustion tube after Experiment II. Similar observations for oil recovery were reported by Chicuta and Trevisan (2009).

Figure 14. Oil breakthrough during Experiment II

The oil recovery comparisons are given in Figure 15. The best recovery (around 83%) was achieved during Experiment V with 53.02% IOS, although the value for Experiment IV with 42.19% IOS is almost the same.

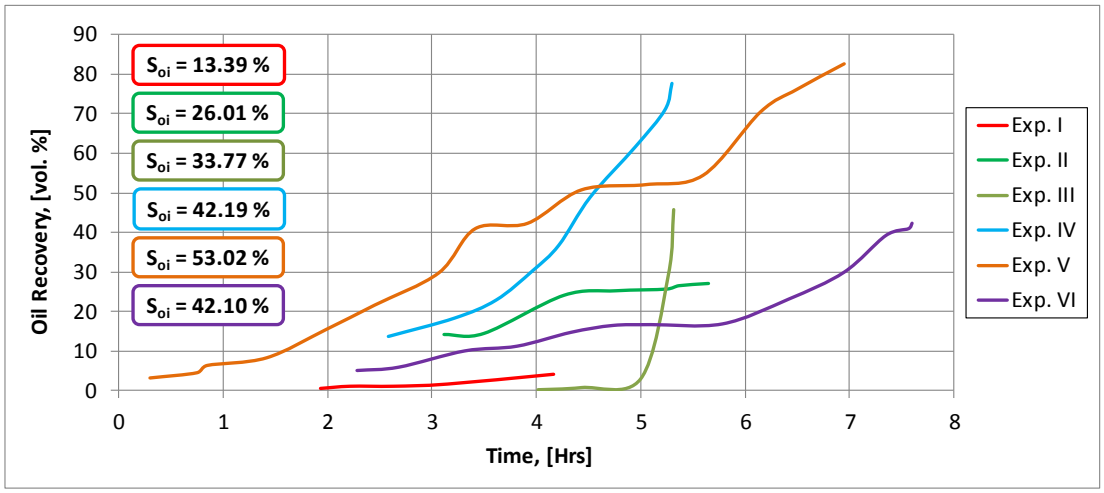

Figure 15. Oil recovery comparisons for all experiments in volume %

Ultimate oil recovery, which was obtained by the end of each experiment, is listed in Table 13. The time required for combustion front to reach a fixed position (around 73.5 cm below from top) after the start of air injection and the cumulative oil recovery by the end of this time are also mentioned in the Table 13.

Table 13. Oil recoveries

Parameters, units	Experiments					
	I	II	III	IV	V	VI
Ultimate Oil Recovery, vol. %	4.1	27.1	45.8	77.7	82.6	42.3
Combustion Front Position, cm	-	73.66	73.66	73.5	73.5	73.5
Time, hrs	-	4.91	4.96	4.45	4.71	6.34
Oil Recovery, vol. %	-	25.5	2.9	47	51.5	22.3

Before oil bank reached the production line during Experiment V, foam production was observed (Figure 16). Foamy oil is usually noted during cold heavy oil production with sand (CHOPS), where evolution of gas from heavy oils results in a bubble phase (Pan et al., 2010).

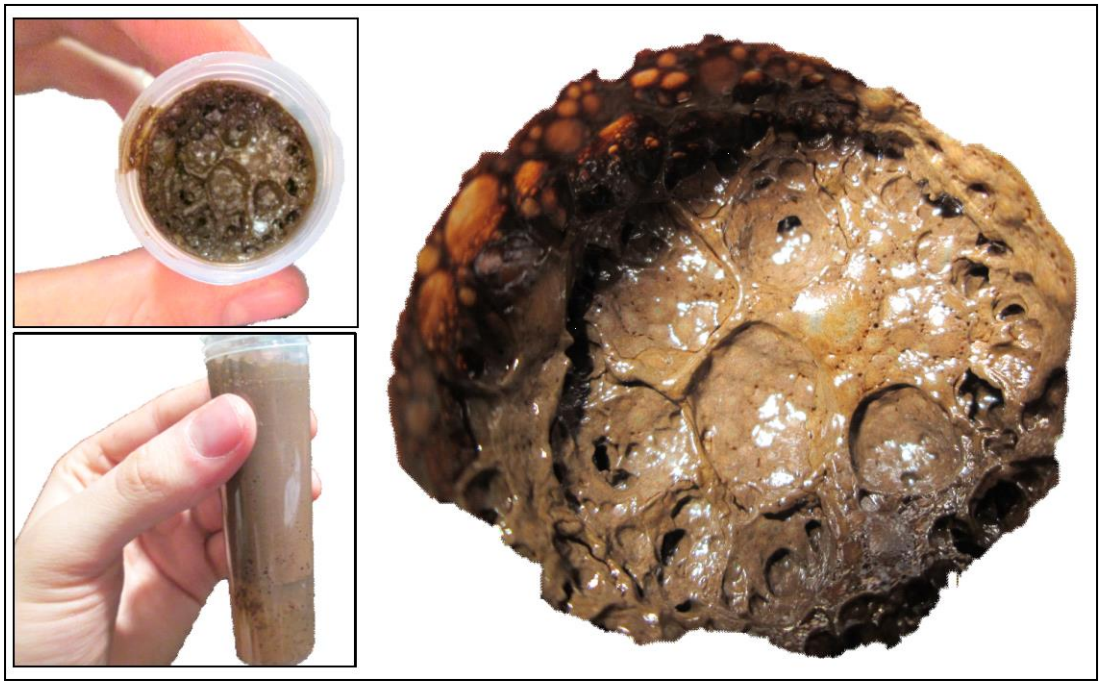

Figure 16. Foam production during Experiment V

Material Balance

Material balance is achieved with the following basic equation:

$$[Mass\ in]_{\ before\ and\ during\ experiment} = [Mass\ out]_{\ after\ experiment}$$

Combustion tube is packed for each experiment with sand (85 ωt %), clay (15 ωt %), water (around 35 vol. %) and different oil saturations (13.39 to 53.02 vol. %).

The mass of this initial sample together with the mass of O_2 injected during the experiment are combined in the left part of the material balance equation. The right part of the equation consists of postmortem mass, total mass of all samples including condensate fluids, mass of produced gases, and mass losses that appeared during postmortem analysis. These constituents for all experiments are given in Table 14.

In Table 14 masses were measured with a weighting machine, except for the injected oxygen that was calculated from air injection rate and with compressibility equation of state, and the total gas produced, which was derived from the material balance equation described above.

Table 14. Mass balance comparison

Parameters, units	Experiments					
	I	II	III	IV	V	VI
Experiment Time, min	258	348	327	324	415	456
Sample Packed, gr	7404.8	8034.6	7941.3	8052.3	8552.2	8142.9
Total O_2 Injected, gr	1893.3	2552.0	2093.7	1934.2	2854.7	3344.0
Postmortem, gr	7060.8	7215.8	7112.9	6997.3	7311.0	7121.5
Total Sampling, gr	309.3	750.1	733.3	983.4	1084.1	842.3
Total Losses, gr	8.2	-	-	35.1	-	-
Total Gas Produced, gr	1919.8	2620.7	2188.8	1970.7	3011.8	3523.1

CT Scan Results

Due to the nature of the ISC, a huge amount of energy is created at the combustion front (Breston, 1958). Under high temperature, thermal expansion of gases takes place. The interaction between these gases and porous media coated with fuel

result in rearrangement of unconsolidated sand and clay particles. This rearrangement changes the permeability and porosity distribution of the medium ahead of the combustion front and affects the process performance. To visualize this effect, after each experiment X-ray computed tomography (CT) scanning was applied on postmortems.

Figure 17 shows postmortem pictures along with cross sectional CT images and the distribution of average CT numbers. Pictures that were obtained close to the ends of combustion tube don't give proper information about CT numbers due to X-artifacts created by combustion tube caps and flanges. One of these artifacts can be noted for the first cross-sectional image of Experiment I (Figure 17). Cross-sectional images for each experiment shown in Figure 17 and marked with red arrows are selected according to the postmortem zones given in Figure 8. Cross-sectional images marked with green arrows represent additional slices along the sand pack.

Voids can be noted for each experiment, but to different extents. Thus, Experiment III is affected mostly by gas thermal expansion, followed by Experiment I, VI, IV, II and V respectively. Stable propagation of combustion front during Experiment III provides evidence that void zones doesn't result in failure of ISC, but affects it performance. Thus, color changes of postmortems are observed in Experiments I, III and IV for positions, where thick void zones appeared in front of combustion front. Particularly, the color of postmortem of Experiment I became darker at 16 cm below from top, where a void zone appeared (Figure 17). This can be considered as the reason of ISC failure for 13.39% IOS case. But it should be also noted that combustion front reached the same temperatures at 26, 30.3 and 36.8 cm below from the air injection point

(Figure 4). This indicates that the ISC failure for 13.39% IOS should be attributed not to the void, but to insufficient amounts of fuel formed.

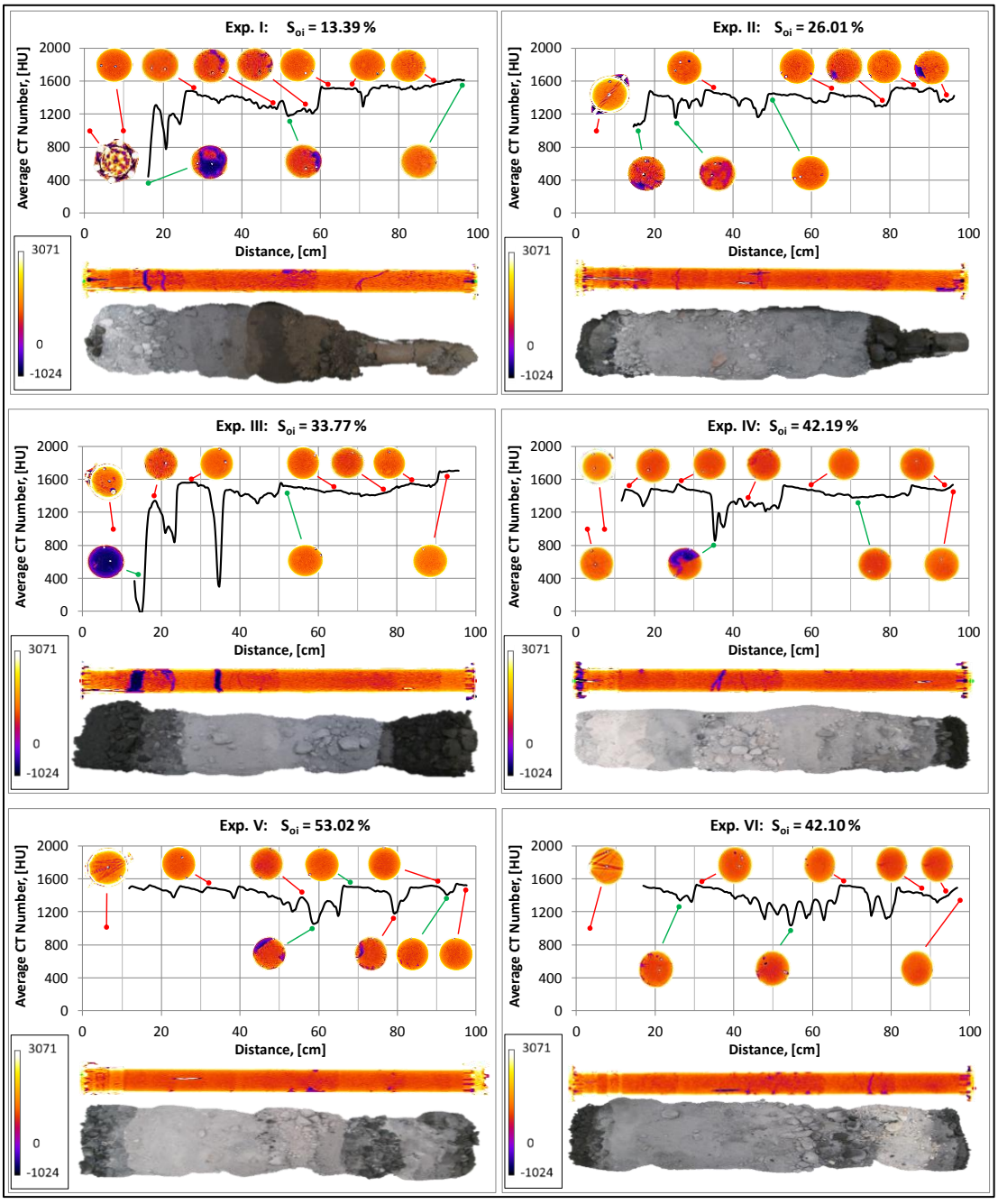

Figure 17. Average CT numbers along the combustion tube for all experiments

CT cross-sectional images can support and enhance the interpretation of combustion tube experimental results.

From temperature profiles (Figure 4) it is observed that Experiment VI despite 42.10% IOS exhibit lower combustion front temperatures than Experiments III to V. A possible reason for this mismatch can be identified with the CT cross-sectional image of postmortem of Experiment VI (Figure 18). In addition to the inserted thermowells two more holes were revealed at different locations. These holes were created due to the necessity of replacement of thermowell fitting that was discovered damaged during the leak test. These two artificially created fractures provided easy pathways through the sand pack, resulted in combustion front breakthroughs and changed the performance of the ISC process.

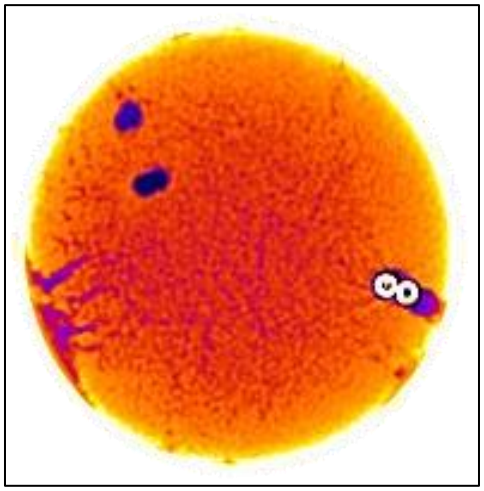

Figure 18. Cross-sectional image of postmortem of Experiment VI
(54 cm below from top)

In Experiment II, combustion front fingering was also observed. However, only one additional penetration of the thermowell was made. Although this fracture has disappeared at the center of the tube by the end of experiment, it remained present at the bottom (Figure 19). Created fracture caused some errors in analytical calculations and therefore, achieved values were ignored.

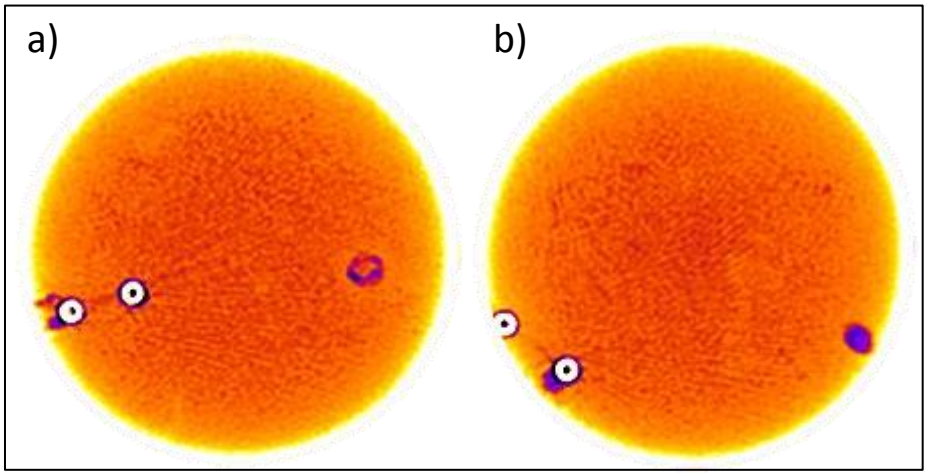

Figure 19. Cross-sectional images of postmortem of Experiment II:
a) 50.7 cm below from top; b) 64.8 cm below from top

Produced gas composition graphs (Figure 6), where large fluctuations took place, can be interpreted properly with CT data as well. These disturbances should be attributed to voids that are common for all six experiments and that can be traced precisely by CT number charts (Figure 17). After each zone the continuity of the combustion front breaks and its performance changes: oxygen uptake lowers and results in increased oxygen amounts in produced gases. This interruption leads to an additional time requirement to reestablish stability of the combustion front. This behavior can be illustrated, for

instance, with Experiment III and a void that is situated at around 33 cm (Figure 17). Combustion front approached this void zone three hours later after the air injection started (Figure 9). Exactly at the same time a sharp rise in the oxygen concentration of produced gases is observed for Experiment III (Figure 6). Similar fluctuations, but less sharp and related to packing heterogeneities, were observed in gas profiles during experiments of Hascakir et al. (2011a).

If combustion front passes the void zone during the transition period of combustion process, then, taking into account previous discussion, stabilization time will be increased. Thus, in Figure 20 Experiment III doesn't fit into increasing trend of stabilization time for Experiments II, IV, and V. This results from the void zone, which appeared during Experiment III at around 13 centimeters below from the top of combustion tube (Figure 17). Experiment VI is omitted because of the longitudinal fractures that resulted in increased oxygen demand (Johnson and Romanovski, 1987). Shortage of oxygen prevented the combustion front from quick establishment of the stability.

Peace River in general requires more time till stabilization of the combustion front than heavy oils mentioned in literature. Thus, 67 minutes was required for 8.65°API Venezuelan crude oil to stabilize with 34% initial oil and 0% water saturation (Hascakir et al., 2011a). Same experiment, but with 34% of water showed almost instantaneous establishment of stable state. The minimum stabilization time for Peace River was 82 min, which was observed during Experiment II that had 26.01% initial oil and 34.96% initial water saturations.

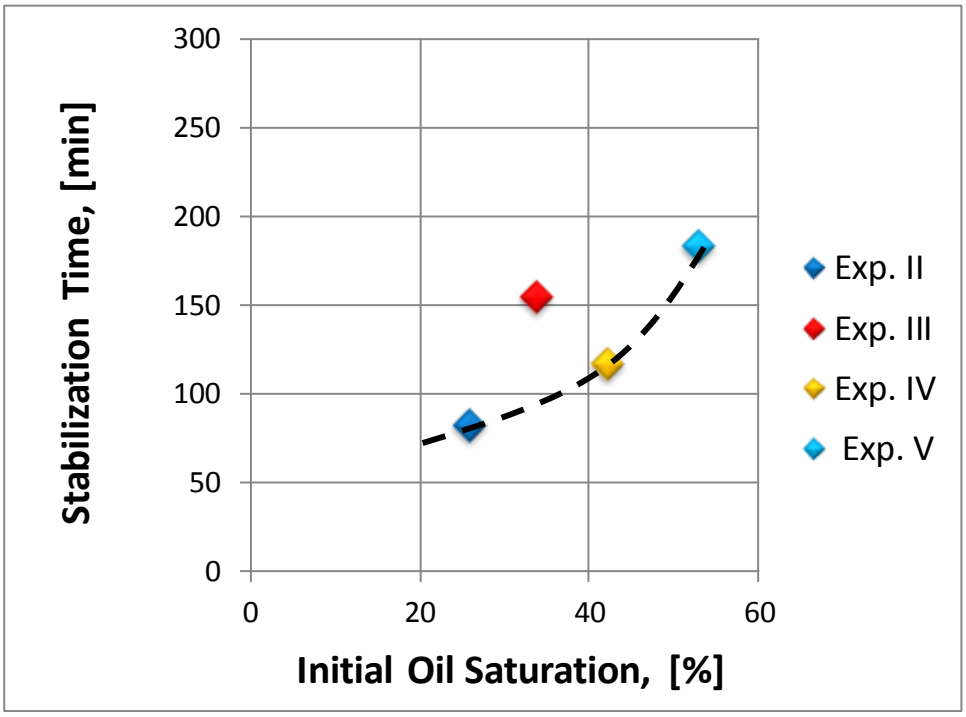

Figure 20. Combined stabilization times

In-Situ Upgrading

To investigate the degree of bitumen upgrading with ISC, viscosity and gravity were measured at different temperatures before and after Experiment III. Viscosity of upgraded oil measured at room temperature was 133 times less than the original bitumen at the same conditions (Figure 21). API gravity was enhanced from 8.6 to 13°API at room temperature (Figure 22).

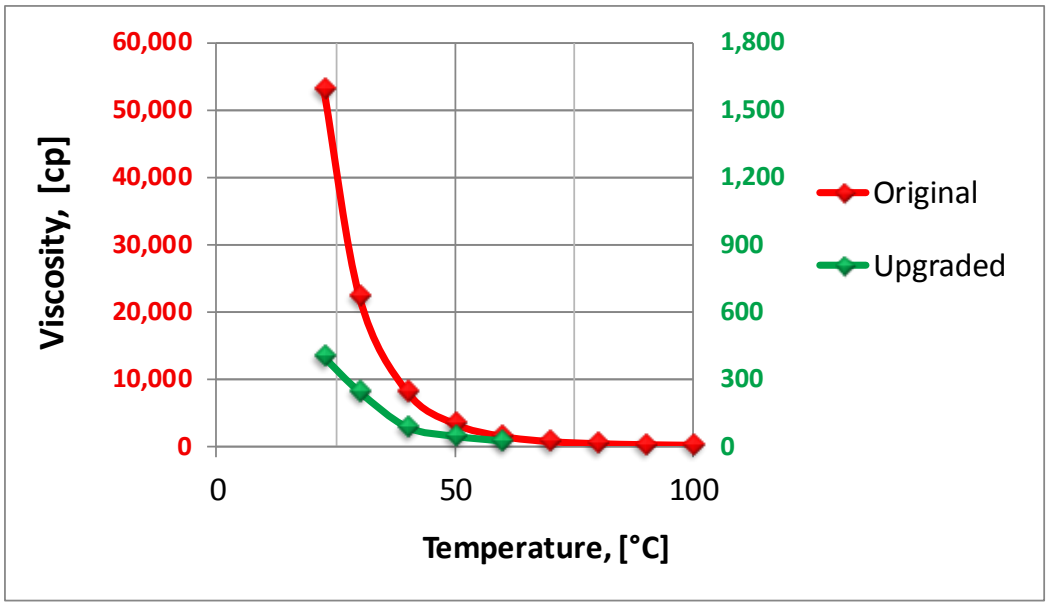

Figure 21. Viscosity change with temperature for bitumen (red curve) and produced oil at the end of Experiment III (green curve)

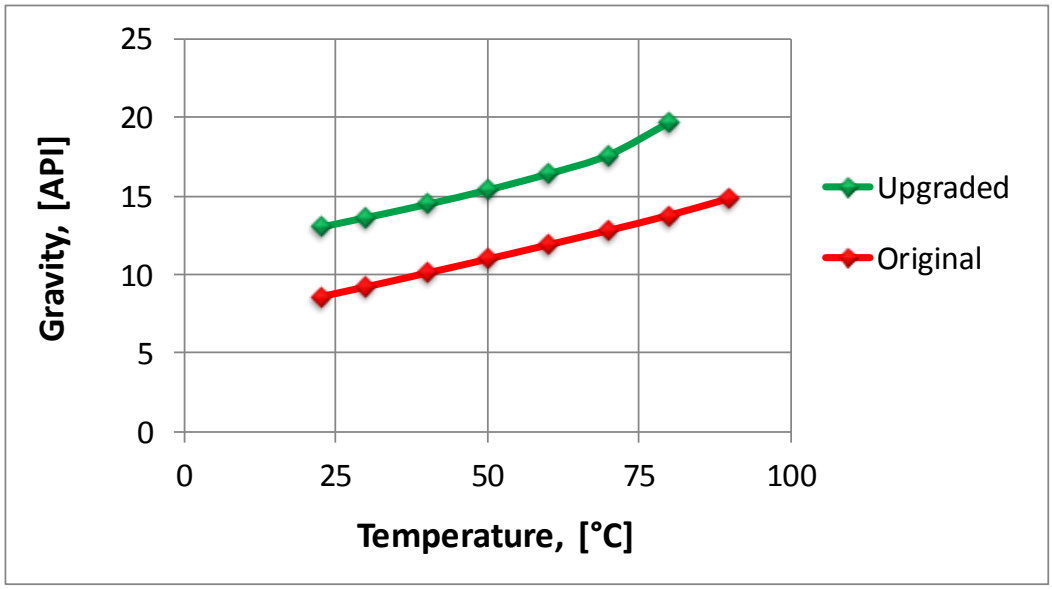

Figure 22. API gravity change with temperature for bitumen (red curve) and produced oil at the end of Experiment III (green curve)

Repeatability of Experiments

Experiment IV with 42.19% IOS was repeated and named Experiment VI. All experimental and initial conditions were kept constant for two experiments. Considering the discussions made in previous sections, Experiment VI reflects the performance of a fractured reservoir. However, temperature profiles of both experiments showed good combustion tube run behavior. This was due to discontinuous, not connected fingerings that were perpendicular to the air injection direction.

Although self-sustained combustion process was achieved during Experiment VI, the performance of ISC was comparatively deteriorated; high experiment time and poor oil recovery were observed. Moreover, literature shows that fractured can result in total failure of a field-scale project (Grosmont oilfield, McDougall et al. (2008)).

CHAPTER IV

CONCLUSION

The following conclusions may be drawn:

- The minimum value of initial oil saturation for self-sustained combustion of Peace River bitumen under 3.4 l/min air injection rate is 26.01%. This implies that a 50% value of IOS shouldn't be a limiting factor during screening of heavy oil reservoirs for In-Situ Combustion.
- The best oxygen utilization and low air requirement during Experiment IV ended with 77.7% oil recovery. Although the highest recovery (82.6%) was noted for the 53.02% IOS case, its combustion front velocity was much slower, than that for 42.19% IOS. This leads to the conclusion, that the best performance of the combustion process was achieved during Experiment IV. This point of conclusion supports the observation of (Ogunbanwo et al., 2012), made with numerical analysis on 10°API gravity oil, that the optimal ISC performance should be observed within IOS values from 45- to 70%.
- Relationships were identified between analytical parameters and initial oil saturation. These correlations, which were achieved through this experimental sensitivity study, are intended to aid the numerical simulation of Peace River bitumen ISC performance.
- ISC is a highly sensitive process. Experiment VI confirms that fractures strongly affect the performance of In-Situ Combustion.

- While fractures that are perpendicular to air injection direction do not change the fate of ISC success, the ones, which are parallel, may cause failure of ISC.
- CT imaging is a valuable tool for interpretation of combustion tube experiments. It minimizes the possibility of misinterpreting conventional results

REFERENCES

Abu-Khamsin, S.A., Brigham, W.E. and Ramey Jr., H.J., 1988. Reaction Kinetics of Fuel Formation for In-Situ Combustion. SPE Reservoir Engineering, 3(4): 1308-1316, SPE-15736-PA.

Agca, C. and Yortsos, Y.C., 1985. Steady-State Analysis of In-Situ Combustion, SPE California Regional Meeting. Society of Petroleum Engineers, Bakersfield, California, SPE-13624-MS.

Akin, S., Kok, M.V., Bagci, S. and Karacan, O., 2000. Oxidation of Heavy Oil and Their SARA Fractions: Its Role in Modeling In-Situ Combustion, SPE Annual Technical Conference and Exhibition. Society of Petroleum Engineers, Dallas, Texas, SPE-63230-MS.

Al-adasani, A. and Bai, B., 2010. Recent Developments and Updated Screening Criteria of Enhanced Oil Recovery Techniques, International Oil and Gas Conference and Exhibition in China. Society of Petroleum Engineers, Beijing, China, SPE-130726-MS.

Alberta Geological Survey, 2012. Alberta Oil Sands, http://www.ags.gov.ab.ca/energy/oilsands/, Accessed: April 10.

Alexander, J.D., Martin, W.L. and Dew, J.N., 1962. Factors Affecting Fuel Availability and Composition During In Situ Combustion, SPE Production Research Symposium, Tulsa, Oklahoma.

Armento, M.E. and Miller, C.A., 1977. Stability of Moving Combustion Fronts in Porous Media. Society of Petroleum Engineers Journal, 17(6): 423-430, SPE-6168-PA.

Bailey, H.R. and Larkin, B.K., 1959. Conduction-Convection in Underground Combustion, AIChE-SPE Joint Symposium, San Francisco, SPE-1482-G.

Bayliss, P. and Levinson, A.A., 1976. Mineralogical Review of the Alberta Oil Sand Deposits (Lower Cretaceous, Mannville Group). Bulletin of Canadian Petroleum Geology, 24(2): 211-224.

Belgrave, J.D.M., Moore, R.G., Ursenbach, M.G. and Bennion, D.W., 1993. A Comprehensive Approach to In-Situ Combustion Modeling. SPE Advanced Technology Series, 1(1): 98-107, SPE-20250-PA.

Benham, A.L. and Poettman, F.H., 1958. The Thermal Recovery Process - An Analysis of Laboratory Combustion Data. Journal of Petroleum Technology, 10(9): 83-85, SPE-1022-G.

Boberg, T.C., 1988. Thermal Methods of Oil Recovery. John Wiley & Sons Ltd, New York, 411 pp.

Bourdarot, G. and Ghedan, S.G., 2011. Modified EOR Screening Criteria as Applied to a Group of Offshore Carbonate Oil Reservoirs, SPE Reservoir Characterisation and Simulation Conference and Exhibition. Society of Petroleum Engineers, Abu Dhabi, UAE, SPE-148323-MS.

Breston, J.N., 1958. Oil Recovery by Heat From In Situ Combustion. Journal of Petroleum Technology: 13-17, SPE-1087-G.

Brigham, W.E., Satman, A. and Soliman, M.Y., 1980. Recovery Correlations for In-Situ Combustion Field Projects and Application to Combustion Pilots. Journal of Petroleum Technology, 32(12): 2132-2138, SPE-7130-PA.

Buchwald Jr., R.W., Hardy, W.C. and Neinast, G.S., 1973. Case Histories of Three In-Situ Combustion Projects. Journal of Petroleum Technology, 25(7): 784-792, SPE-3781-PA.

Burger, J.G. and Sahuquet, B.C., 1972. Chemical Aspects of In-Situ Combustion - Heat of Combustion and Kinetics. Society of Petroleum Engineers Journal, 12(5): 410-422, SPE-3599-PA.

Castanier, L.M. and Brigham, W.E., 2003. Upgrading of Crude Oil via In Situ Combustion. Journal of Petroleum Science and Engineering, 39(1–2): 125-136.

Chicuta, A.M. and Trevisan, O.V., 2009. Experimental Study on In-Situ Combustion of a Brazilian Heavy Oil, Latin American and Caribbean Petroleum Engineering Conference. Society of Petroleum Engineers, Cartagena de Indias, Colombia, SPE-122036-MS.

Chu, C., 1963. Two-Dimensional Analysis of a Radial Heat Wave, SPE Production Research Symposium, U. of Oklahoma, Norman, Oklahoma, SPE-560-PA.

Chu, C., 1982. State-of-the-Art Review of Fireflood Field Projects (includes associated papers 10901 and 10918). Journal of Petroleum Technology, 34(1): 19-36, SPE-9772-PA.

Earlougher Jr., R.C., Galloway, J.R. and Parsons, R.W., 1970. Performance of the Fry In-Situ Combustion Project. Journal of Petroleum Technology: 551-557, SPE-2409-PA.

Freitag, N.P. and Verkoczy, B., 2005. Low-Temperature Oxidation of Oils in Terms of SARA Fractions: Why Simple Reaction Models Don't Work. Journal of Canadian Petroleum Technology, 44(3), PETSOC-05-03-05.

Glatz, G., 2012. Towards Field Scale In-Situ Combustion Simulation, Stanford University, 87 pp, https://pangea.stanford.edu/ERE/pdf/pereports/MS/Glatz2012.pdf, Accessed: April 17, 2013.

Greaves, M. et al., 2000. Air Injection into Light and Medium Heavy Oil Reservoirs: Combustion Tube Studies on West of Shetlands Clair Oil and Light Australian Oil. Chemical Engineering Research and Design, 78(5): 721-730.

Gutierrez, D., Skoreyko, F., Moore, R.G., Mehta, S.A. and Ursenbach, M.G., 2009. The Challenge of Predicting Field Performance of Air Injection Projects Based on Laboratory and Numerical Modelling. Journal of Canadian Petroleum Technology, 48(4): 23-33, PETSOC-09-04-23-DA.

Hamm, R.A. and Ong, T.S., 1995. Enhanced Steam-assisted Gravity Drainage: A New Horizontal Well Recovery Process For Peace River, Canada. Journal of Canadian Petroleum Technology, 34(4), PETSOC-95-04-03.

Hascakir, B., Glatz, G., Castanier, L.M. and Kovscek, A., 2011a. In-Situ Combustion Dynamics Visualized With X-Ray Computed Tomography. SPE Journal, 16(3): pp. 524-536, SPE-135186-PA.

Hascakir, B., Ross, C.M., Castanier, L.M. and Kovscek, A.R., 2011b. Fuel Formation During In-Situ Combustion of Heavy Oil, SPE Annual Technical Conference and Exhibition. Society of Petroleum Engineers, Denver, Colorado, SPE-146867-MS.

Islam, M.R., Chakma, A. and Farouq Ali, S.M., 1989. State-of-the-Art of In-Situ Combustion Modeling and Operations, SPE California Regional Meeting. 1989 Copyright 1989, Society of Petroleum Engineers, Inc., Bakersfield, California, SPE-18755-MS.

Johnson, L.A. and Romanovski, L.J., 1987. Evaluation of Steasm-to-Oxygen Ratios for Forward Combustion in Asphalt Ridge Tar Sand, Western Research Institute, http://www.netl.doe.gov/kmd/cds/disk44/K-Thermal%20Recovery/doemc11076-2441.PDF, Accessed: April 7, 2013.

Kok, M.V. and Bagci, S., 2004. Characterization and Kinetics of Light Crude Oil Combustion in the Presence of Metallic Salts. Energy & Fuels, 18(3): 858-865.

Kok, M.V. and Karacan, C.O., 1997. Behavior and Effect of SARA Fractions of Oil During Combustion, International Thermal Operations and Heavy Oil Symposium. Society of Petroleum Engineers, Bakersfield, California, SPE-37559-MS.

Koottungal, L., 2008. Worldwide EOR Survey, Oil & Gas Journal, http://www.ogj.com/articles/print/volume-106/issue-15/drilling-production/special-report-2008-worldwide-eor-survey.html, Accessed: April 7, 2013.

Labastie, A., 2011. Increasing Recovery Factors: A Necessity. JPT, 63(8): 12-13.

Martin, W.L., Alexander, J.D. and Dew, J.N., 1957. Process Variables of In Situ Combustion, 32nd Annual Fall Meeting of Society of Petroleum Engineers, Dallas, Texas, SPE-914-G.

McDougall, J., Alvarez, J.M. and Isaacs, E., 2008. Alberta Carbonates - the Third Trillion. World Petroleum Congress, WPC-19-0925.

Millour, J.P., Moore, R.G., Bennion, D.W., Ursenbach, M.G. and Gie, D.N., 1985. A Simple Implicit Model for Thermal Cracking of Crude Oils, SPE Annual Technical Conference and Exhibition. Society of Petroleum Engineers, Las Vegas, Nevada, SPE-14226-MS.

Moore, R.G., Ursenbach, M.G., Laureshen, C.J., Belgrave, J.D.M. and Mehta, S.A., 1999. Ramped Temperature Oxidation Analysis of Athabasca Oil Sands Bitumen. Journal of Canadian Petroleum Technology, 38(13), PETSOC-99-13-40.

Murugan, P., Mahinpey, N., Mani, T. and Freitag, N., 2009. Pyrolysis and Combustion Kinetics of Fosterton Oil Using Thermogravimetric Analysis. Fuel, 88(9): 1708-1713.

Nelson, T.W. and McNeil, J.S., 1961. How to Engineer an In-Situ Combustion Project. Oil & Gas Journal, 59(23): 58-65.

Ogunbanwo, O.O., Gerritsen, M.G. and Kovscek, A.R., 2012. Uncertainty Analysis on In-Situ Combustion Simulations Using Experimental Design, SPE Western Regional Meeting. Society of Petroleum Engineers, Bakersfield, California, SPE-153887-MS.

Onishi, T., Teramoto, T. and Okatsu, K., 2006. History Matching With Combustion-Tube Tests for Light-Oil Air-Injection Project, International Oil & Gas Conference and Exhibition in China. Society of Petroleum Engineers, Beijing, China, SPE-103848-MS.

Pan, Y. et al., 2010. Research Progress of Modelling on Cold Heavy Oil Production with Sand, SPE Western Regional Meeting. Society of Petroleum Engineers, Anaheim, California, SPE-133587-MS.

Paszkiewicz, L., 2012. Extra Heavy Oils in the World Energy Supply, Canada, http://www.total.com/MEDIAS/MEDIAS_INFOS/5776/FR/EXTRA_HEAVY_OILS_IN_THE_WORLD_ENERGY_SUPPLY.pdf, Accessed: April 13.

Penberthy, W.L., Berry, H.J. and Ramey, H.J., 1968. Some Fundamentals of Steam-Plateau Behavior in Combustion Oil Recovery, 43d Annual Fall Meeting of the Society of Petroleum Engineers of AIME, Houston, Texas, SPE-2213-MS.

Penberthy, W.L. and Ramey, H.J., 1965. Design and Operation of laboratory Combustion Tubes, SPE Annual Fall Meeting, Denver, Colorado, SPE-1290-PA.

Rahnema, H., Barrufet, M. and Mamora, D.D., 2012. Self-Sustained CAGD Combustion Front Development; Experimental and Numerical Observations, SPE Improved Oil Recovery Symposium. Society of Petroleum Engineers, Tulsa, Oklahoma, SPE-154333-MS.

Ramey, H.J., 1958. Transient Heat Conduction During Radial Movement of a Cylindrical Heat Source - Applications to the Thermal Recovery Process, 33rd Annual Fall Meeting of Society of Petroleum Engineers, Houston, Texas, SPE-1133-G.

Regtien, J.M.M., 2010. Extending The Smart Fields Concept To Enhanced Oil Recovery, SPE Russian Oil and Gas Conference and Exhibition. Society of Petroleum Engineers, Moscow, Russia, SPE-136034-MS.

Ren, Y., Freitag, N.P. and Mahinpey, N., 2005. A Simple Kinetic Model for Coke Combustion During an In Situ Combustion (ISC) Process, Canadian International Petroleum Conference. Petroleum Society of Canada, Calgary, Alberta, PETSOC-2005-110.

Rodriguez, J.R. and Mamora, D.D., 2005. Analytical Model of the Combustion Zone in Oxygen-Enriched In Situ Combustion Tube Experiments, Canadian International Petroleum Conference. Petroleum Society of Canada, Calgary, Alberta, PETSOC-2005-072.

Rojas, L.A., 2011. Technologias de Crudos Pesados, Bogota, Colombia, Conference Proceedings.

Sarathi, P.S., 1998. In-Situ Combustion Handbook - Principles and Practices. U.S. Department of Energy, Tulsa, Oklahoma, 403 pp.

Sen, M.K. and Vedanti, N., 2008. Prestack Seismic Inversion Tracks In Situ Combustion: 4D Seismic at the Balol Field, India, SPE Annual Technical Conference and Exhibition. Society of Petroleum Engineers, Denver, Colorado, SPE-116600-MS.

Sibbald, L.R., Moore, R.G. and Bennion, D.W., 1991. In-Situ Combustion Process Study With a Combined Experimental/Analytical Approach. SPE Reservoir Engineering, 6(3): 295-302, SPE-18074-PA.

Taber, J.J., Martin, F.D. and Seright, R.S., 1997. EOR Screening Criteria Revisited - Part 1: Introduction to Screening Criteria and Enhanced Recovery Field Projects. SPE Reservoir Engineering, 12(3): 189-198, SPE-35385-PA.

Thomas, G.W., 1963. A Study of Forward Combustion in a Radial System Bounded by Permeable Media, SPE Annual Fall Meeting, New Orleans, Texas, SPE-681-PA.

Turta, A.T., Lu, J., Bhattacharya, R.N., Condrachi, A. and Hanson, W., 2005. Current Status of the Commercial In Situ Combustion (ISC) Projects and New Approaches to Apply ISC, Canadian International Petroleum Conference. Petroleum Society of Canada, Calgary, Alberta, PETSOC-2005-002.

Verkoczy, B., 1993. Factors Affecting Coking in Heavy Oil Cores, Oils and SARA Fractions Under Thermal Stress. Journal of Canadian Petroleum Technology, 32(7): 25-33, PETSOC-93-07-02.

Vogel, L.C. and Krueger, R.F., 1955. An Analog Computer for Studying Heat Transfer During a Thermal Recovery Process, Petroleum Branch Fall Meeting, New Orleans, Texas, SPE-534-G.

Xia, T.X. and Greaves, M., 2001. Downhole Upgrading Athabasca Tar Sand Bitumen Using THAI - SARA Analysis, SPE International Thermal Operations and Heavy Oil Symposium. Society of Petroleum Engineers Inc., Porlamar, Margarita Island, Venezuela, SPE-69693-MS.

Xia, T.X. and Greaves, M., 2002. Upgrading Athabasca Tar Sand Using Toe-to-Heel Air Injection. Journal of Canadian Petroleum Technology, 41(8), PETSOC-02-08-02.

Xu, H.H. et al., 2000. In Situ Upgrading of Heavy Oil, Canadian International Petroleum Conference. Petroleum Society of Canada, Calgary, Alberta, PETSOC-2000-030.

APPENDIX A

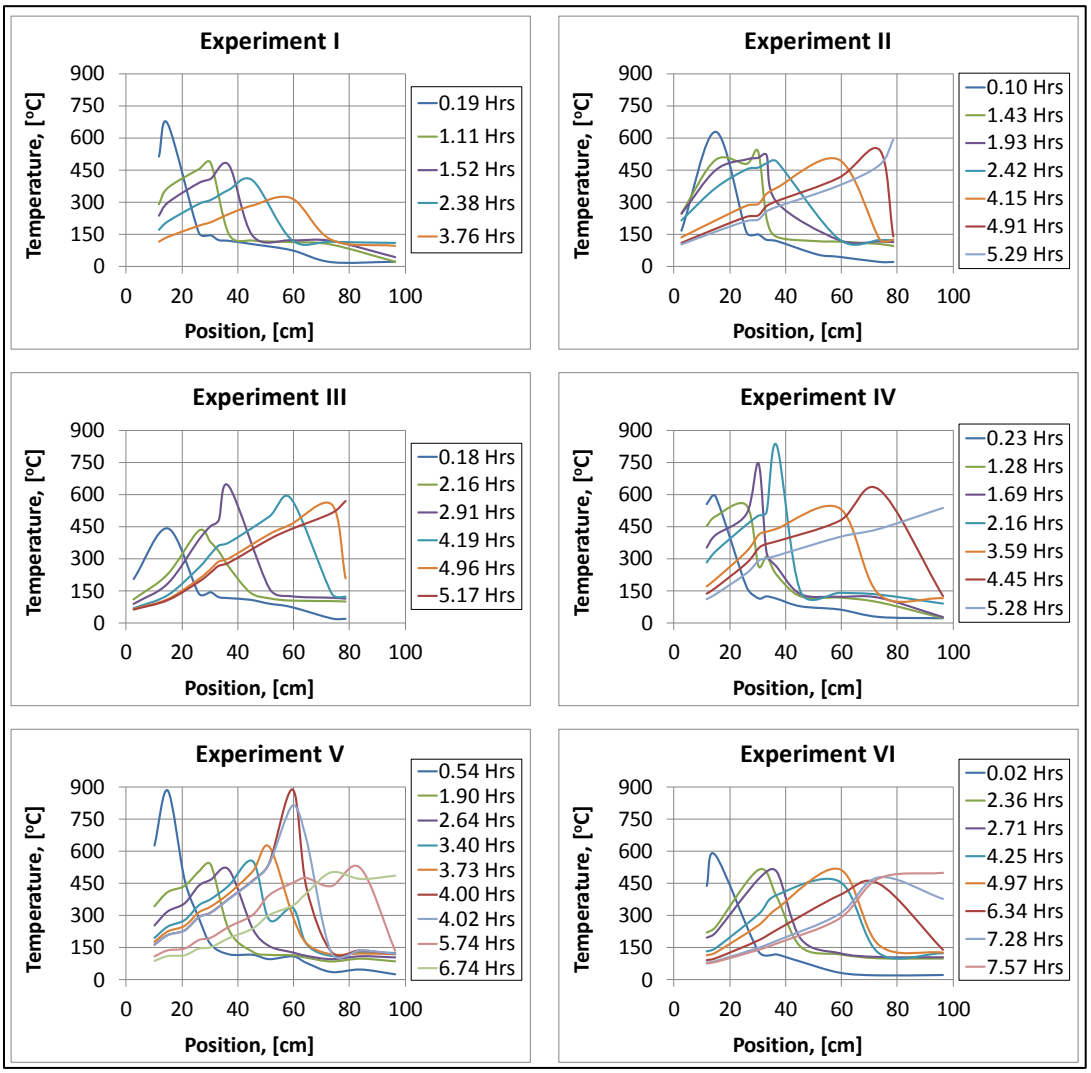

Figure 23. Temperature profiles for all experiments

APPENDIX B

The methodology of sample preparation includes the following calculations, measurements and procedures:

1) Porosity measurement:

   A mixture of sand (84 ωt.%) and clay (84 ωt.%) was placed into a measuring cylinder. Further, fixed volume of water was added. On the next day the porosity was calculated from the following formula:

$$\emptyset = \frac{V_1 - V_2}{V_{sand\ and\ clay}}$$

   where V_1 is the volume of added water and V2 is the volume of water that remained above the mixture of sand and clay after one day of gravity drainage.

   A value of 32% porosity was measured.

2) Volume of combustion tube, cm^3:

$$V_{CT} = \frac{\pi D_{CT}^2}{4} L_{CT}$$

   where D_{CT} and L_{CT} are the inner diameter and length of the combustion tube accordingly (cm^3)

$$V_{CT} = \frac{3.1415 * 7.3^2}{4} * 101.2 = 4235.5\ cm^3 \approx 4235.5\ ml$$

3) Pore volume for sand pack, ml:

$$V_{pv} = V_{CT}\,\emptyset$$

$$V_{pv} = 4235.5 * 0.32 = 1355.36\ ml$$

4) The amounts of sand, clay, oil and water were weighted. After the sample was mixed for three hours by hands to reach the homogeneous mixture. Further, sample was packed and the rest (unpacked sample) was weighted. Achieved values of initial oil and water saturations are listed in Table 15. Uncertainty of mass of packed sample is expected not to exceed 1% (75 gr).

Table 15. Parameters measured and calculated during sample preparation

Parameters, units		Experiments					
		I	II	III	IV	V	VI
Total Sand, gr		7546	7546	7546	7546	7546	7546
Total Clay, gr		970	970	970	970	970	970
Total Water, gr		560	560	560	560	560	560
Total Oil, gr		230	420	560	700	840	690
Total Sample, gr		9306	9496	9636	9776	9916	9766
Packed Sample, gr		7404.8	8034.6	7941.3	8052.3	8552.2	8142.9
Share of Packed Sample, %		79.57	84.61	82.41	82.37	86.25	83.38
Water Packed	gr	445.6	473.8	461.5	461.3	483.0	466.9
	ml	445.6	473.8	461.5	461.3	483.0	466.9
Oil Packed	gr	183.0	355.4	461.5	576.6	724.5	575.3
	ml	181.5	352.5	457.8	571.9	718.6	570.6
Initial Water Saturation		32.88	34.96	34.05	34.03	35.63	34.45
Initial Oil Saturation		13.39	26.01	33.77	42.19	53.02	42.10

Density of Peace River bitumen was measured to be equal 1008.2 kg/m^3 at room temperature. Water density was assumed as 1000 kg/m^3.

5) Initial oil and water saturations that are listed in Table 15 were calculated with the following formulas, vol.%:

$$S_{oi} = \frac{Oil\ Packed, ml}{V_{pv},\ ml}$$

$$S_{wi} = \frac{Water\ Packed, ml}{V_{pv},\ ml}$$

APPENDIX C

During all experiments mole % of O_2, CO_2, CO and CH_4 were measured continuously. Nitrogen in air is assumed inert (Nelson and McNeil, 1968).

Table 16. Laboratory data obtained from Experiment II

Laboratory Data			
Parameters, units		**Symbol**	**Value**
Composition of Injected Air, mol. %	Nitrogen	N_{2i}	79
	Oxygen	O_{2i}	21
Average Gas Composition of Produced Gases, mol.%	Methane	CH_4	0.1739
	Oxygen	O_2	4.8967
	Carbon Dioxide	CO_2	9.4019
	Carbon Monoxide	CO	4.4167
Injected Gas Volume, scf		$V_{i\text{-}lab}$	4.394
Burned Sand Volume, ft^3		$V_{burned\text{-}sand\text{-}lab}$	0.01484

1. Nitrogen concentration in produced gases:

$$N_2 = 100 - (O_2 + CO_2 + CO + CH_4)$$

$$= 100 - (4.8967 + 9.4019 + 4.4167 + 0.1739) = 81.1108\ mol.\%$$

2. Normalization of produced gases for stabilized zone:

$$[O_2] = \frac{O_2 * 100}{O_2 + CO_2 + CO + N_2} = \frac{4.8967 * 100}{4.8967 + 9.4019 + 4.4167 + 81.1108}$$

$$= 4.905\ mol.\%$$

$$[CO_2] = \frac{CO_2 * 100}{O_2 + CO_2 + CO + N_2} = \frac{9.4019 * 100}{4.8967 + 9.4019 + 4.4167 + 81.1108}$$

$$= 9.418\ mol.\%$$

$$[CO] = \frac{CO * 100}{O_2 + CO_2 + CO + N_2} = \frac{4.4167 * 100}{4.8967 + 9.4019 + 4.4167 + 81.1108}$$

$$= 4.425\ mol.\%$$

$$[N_2] = \frac{CO_2 * 100}{O_2 + CO_2 + CO + N_2} = \frac{81.1108 * 100}{4.8967 + 9.4019 + 4.4167 + 81.1108}$$

$$= 81.252\ mol.\%$$

3. H/C ratio:

$$n = \frac{H}{C} = \frac{4\left(\frac{[N_2]}{R} - [CO_2] - \frac{[CO]}{2} - [O_2]\right)}{([CO_2] + [CO])} = \frac{4\left(\frac{81.252}{3.762} - 9.418 - \frac{4.425}{2} - 4.905\right)}{(9.418 + 4.425)}$$

$$= 1.463$$

4. The mole percent ratio of CO over CO_2 is calculated:

$$m = \frac{[CO]}{[CO_2]} = \frac{4.425}{9.418} = 0.4698$$

5. Ratio of mole percent of N_2 to O_2 in the feed gas (injected air):

$$R = \left(\frac{N_2}{O_2}\right)_{feed\ gas} = \frac{79}{21} = 3.762$$

6. Oxygen Utilization:

$$Y = \frac{\frac{[N_2]}{R} - [O_2]}{\frac{[N_2]}{R}} = \frac{\frac{81.252}{3.762} - 4.905}{\frac{81.252}{3.762}} = 0.773$$

7. Stoichiometry of a fuel burning reaction:

$$CH_n + \frac{1}{Y}\left(\frac{2m+1}{2m+2} + \frac{n}{4}\right) O_2 + \frac{R}{Y} \cdot \left(\frac{2m+1}{2m+2} + \frac{n}{4}\right) N_2$$

$$\rightarrow \frac{m}{m+1} CO_2 + \frac{1}{m+1} CO + \frac{1-Y}{Y}\left(\frac{2 \cdot m + 1}{2 \cdot m + 2} + \frac{n}{4}\right) O_2 + \frac{n}{2} H_2O$$

$$+ \frac{R}{Y}\left(\frac{2m+1}{2m+2} + \frac{n}{4}\right) N_2$$

$$CH_{1.463} + \frac{1}{0.773}\left(\frac{2 * 0.4698 + 1}{2 * 0.4698 + 2} + \frac{1.463}{4}\right) O_2 + \frac{3.762}{0.773} \cdot \left(\frac{2 * 0.4698 + 1}{2 * 0.4698 + 2} + \frac{1.463}{4}\right) N_2$$

$$\rightarrow \frac{0.4698}{0.4698 + 1} CO_2 + \frac{1}{0.4698 + 1} CO$$

$$+ \frac{1 - 0.773}{0.773}\left(\frac{2 * 0.4698 + 1}{2 * 0.4698 + 2} + \frac{1.463}{4}\right) O_2 + \frac{1.463}{2} H_2O$$

$$+ \frac{3.762}{0.773}\left(\frac{2 * 0.4698 + 1}{2 * 0.4698 + 2} + \frac{1.463}{4}\right) N_2$$

$$CH_{1.46} + \ 1.327\ O_2 + \ 4.99\ N_2$$

$$\rightarrow 0.32\ CO_2 + 0.68\ CO + 0.301\ O_2 + 0.732\ H_2O + \ 4.99\ N_2$$

8. Oxygen/fuel ratio:

$$\frac{O_2}{Fuel} = \frac{379\,\frac{[N_2]}{R}}{12.011([CO_2]+[CO]) + 4.032\left(\frac{[N_2]}{R} - [CO_2] - \frac{[CO]}{2} - [O_2]\right)}$$

$$= \frac{379 * \frac{81.252}{3.762}}{12.011 * (9.418 + 4.425) + 4.032 * \left(\frac{81.252}{3.762} - 9.418 - \frac{4.425}{2} - 4.905\right)}$$

$$= 43.85\ \frac{\text{scf}}{\text{lbm}}$$

9. Air/Fuel Ratio:

$$\frac{Air}{Fuel} = (1+R)\frac{O_2}{Fuel} = (1+3.762) * 43.85 = 208.81\ \frac{\text{scf}}{\text{lbm}}$$

10. Unreacted O_2 and Produced CO_2 , CO, N_2:

$$Unreacted\ O_2 = \frac{V_{i-lab}\,[O_2]}{[N_2]\,\left(1+\frac{1}{R}\right)} = \frac{5.224 * 4.905}{81.252 * \left(1+\frac{1}{3.762}\right)} = 0.21\ \text{scf}$$

$$Produced\ CO_2 = \frac{V_{i-lab}\,[CO_2]}{[N_2]\,\left(1+\frac{1}{R}\right)} = \frac{5.224 * 9.418}{81.252 * \left(1+\frac{1}{3.762}\right)} = 0.402\ \text{scf}$$

$$Produced\ CO = \frac{V_{i-lab}\,[CO]}{[N_2]\,\left(1+\frac{1}{R}\right)} = \frac{5.224 * 4.425}{81.252 * \left(1+\frac{1}{3.762}\right)} = 0.189\ \text{scf}$$

$$Produced\ N_2 = \frac{V_{i-lab}}{\left(1+\frac{1}{R}\right)} = \frac{5.224}{\left(1+\frac{1}{3.762}\right)} = 3.471\ \text{scf}$$

11. Fuel consumed per volume of sand burned:

$$C\ in\ fuel\ burned = \frac{12}{379}\ (Produced\ CO_2 + Produced\ CO)$$

$$= \frac{12}{379} * (0.402 + 0.189)\ = 0.01871\ \text{lb}$$

$H\ in\ fuel\ burned$

$$= \frac{4}{379}\left(\frac{Produced\ N_2}{R} - Unreacted\ O_2 - Produced\ CO_2 - 0.5\ Produced\ CO\right) = \frac{4}{379} * \left(\frac{3.471}{3.762} - 0.21 - 0.402 - 0.5 * 0.189\right)$$

$$= 0.00228 \text{ lb}$$

$$Total\ weight\ of\ Consumed\ Fuel = C\ in\ fuel\ burned + H\ in\ fuel\ burned$$

$$= 0.01871 + 0.00228 = 0.02099 \text{ lb}$$

$$C_f = \frac{Total\ Weight\ of\ Consumed\ Fuel}{Burned\ Sand\ Volume} = \frac{0.02099}{0.01484} = 1.4144\ \frac{\text{lb}}{\text{ft}^3}$$

12. Air Requirement:

$$X = \frac{2\ Produced\ CO_2 + Produced\ CO}{2\ Produced\ CO_2 + 2\ Produced\ CO} + \frac{\frac{H}{C}ratio}{4} = \frac{2 * 9.418 + 4.425}{2 * 9.418 + 2 * 4.425} + \frac{1.463}{4}$$

$$= 1.206$$

$$K = \frac{(100 - 4.761\ Produced\ O_2)}{\left(100 + \frac{Produced\ O_2}{X} - Produced\ O_2\right)} = \frac{(100 - 4.761 * 4.905)}{\left(100 + \frac{4.905}{1.206} - 4.905\right)} = 0.7729$$

$$A_r = 379.1\ \frac{X\ C_f}{\frac{O_{2i\ feed\ gas}}{100}\ K\ \left(12 + \frac{H}{C}ratio\right)} = 379.1\ \frac{1.206 * 1.4144}{\frac{21}{100} * 0.7729 * (12 + 1.463)}$$

$$= 295.93\ \frac{\text{scf}}{\text{ft}^3}$$

13. Heat of combustion:

$$H_c = \Delta H = \left[\frac{\left(478260 + 356130\ \frac{[CO]}{[CO_2]}\right)}{\left(1 + \frac{[CO]}{[CO_2]}\right)\left(12 + \frac{H}{C}ratio\right)}\right] + \left[\frac{\left(56115\ \frac{H}{C}ratio - 309060\right)}{\left(12 + \frac{H}{C}ratio\right)}\right]$$

$$= \left[\frac{\left(478260 + 356130\ *\ \frac{4.425}{9.418}\right)}{\left(1 + \frac{4.425}{9.418}\right)\ (12 + 1.463)}\right] + \left[\frac{(56115 * 1.463 - 309060)}{(12 + 1.463)}\right]$$

$$= 15{,}766\ \frac{\text{BTU}}{\text{lbm}}$$

APPENDIX D

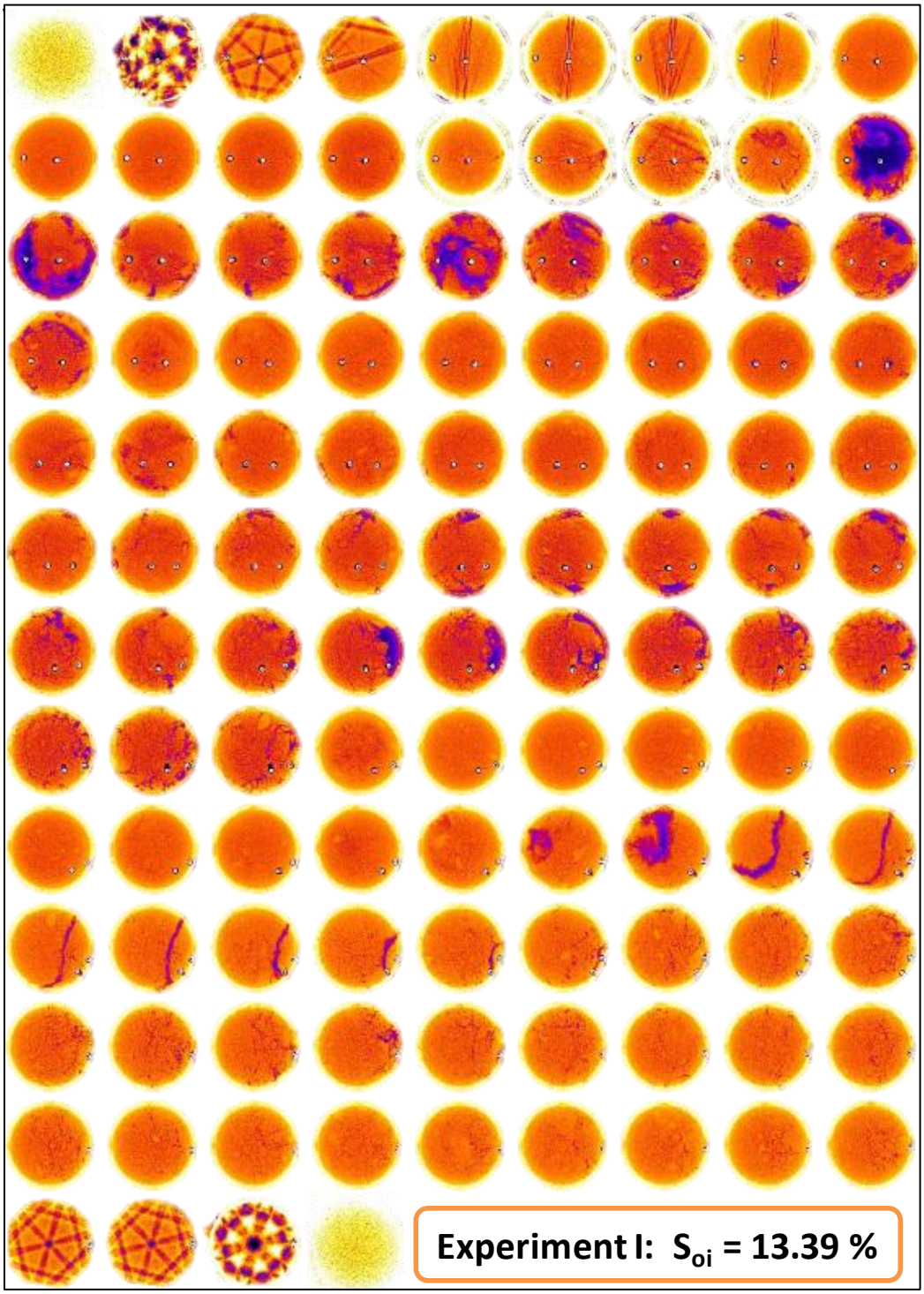

Figure 24. CT cross-sectional images taken after the Experiment I (the image interval is 0.9 cm)

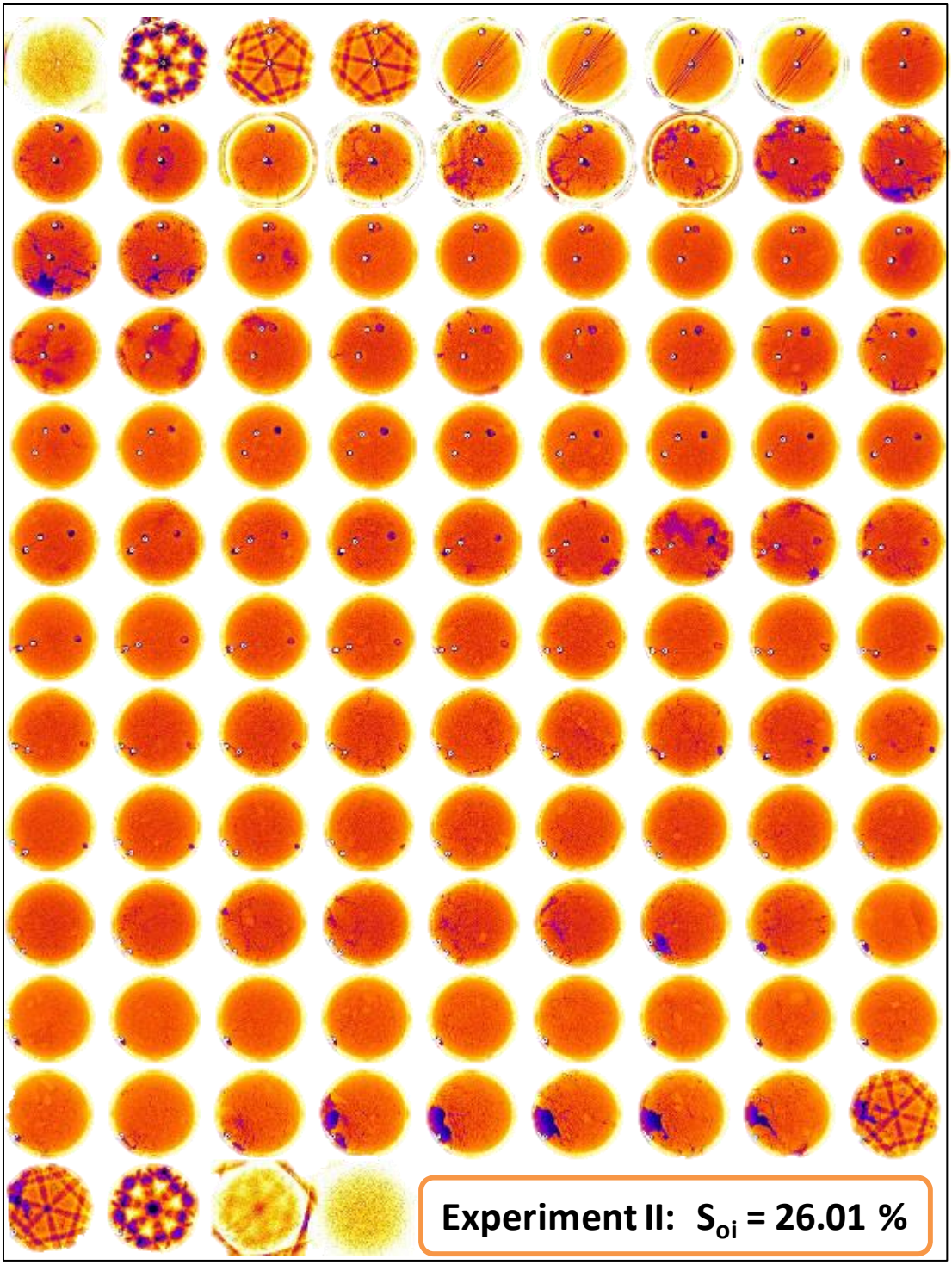

Figure 25. CT cross-sectional images taken after the Experiment II (the image interval is 0.9 cm)

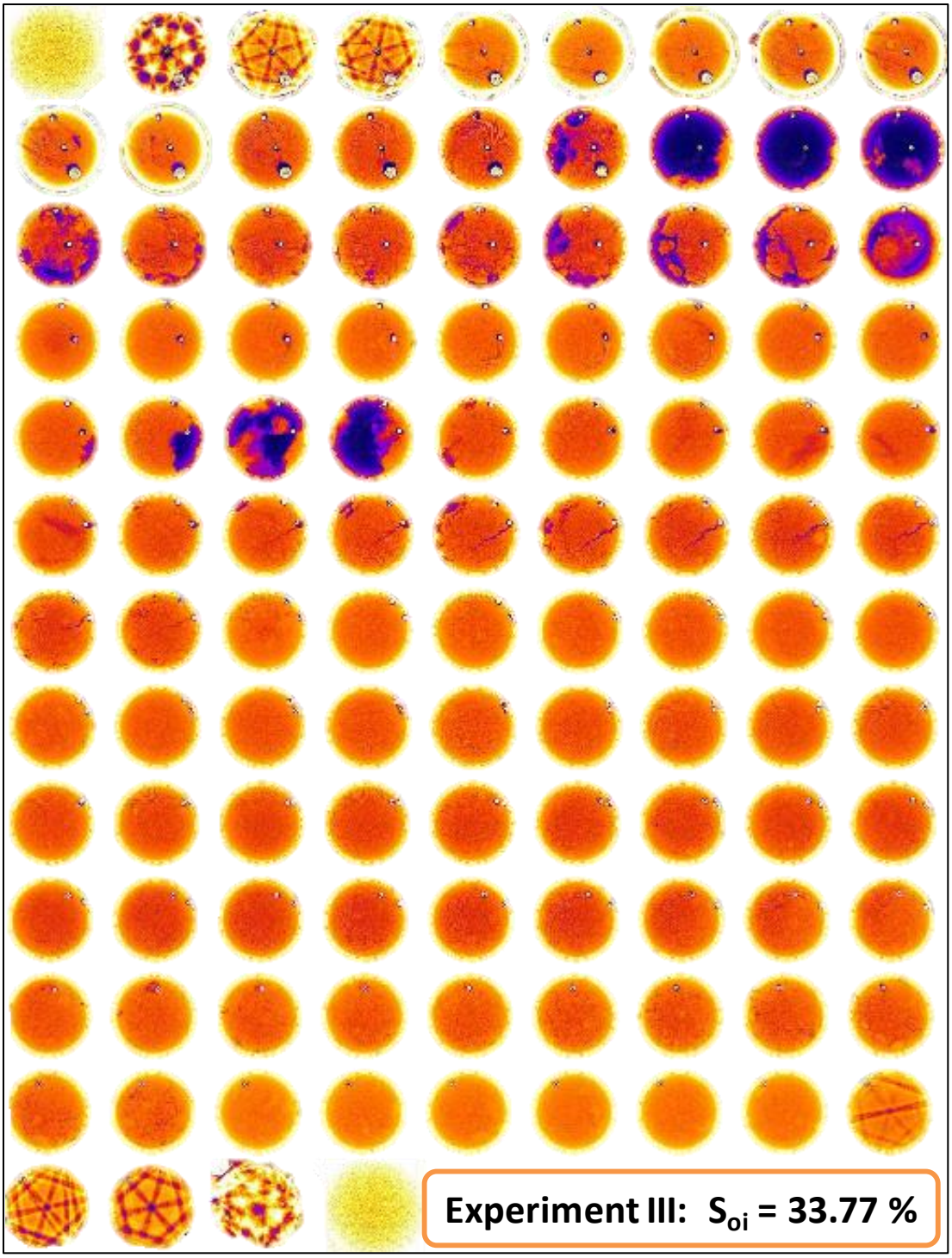

Figure 26. CT cross-sectional images taken after the Experiment III (the image interval is 0.9 cm)

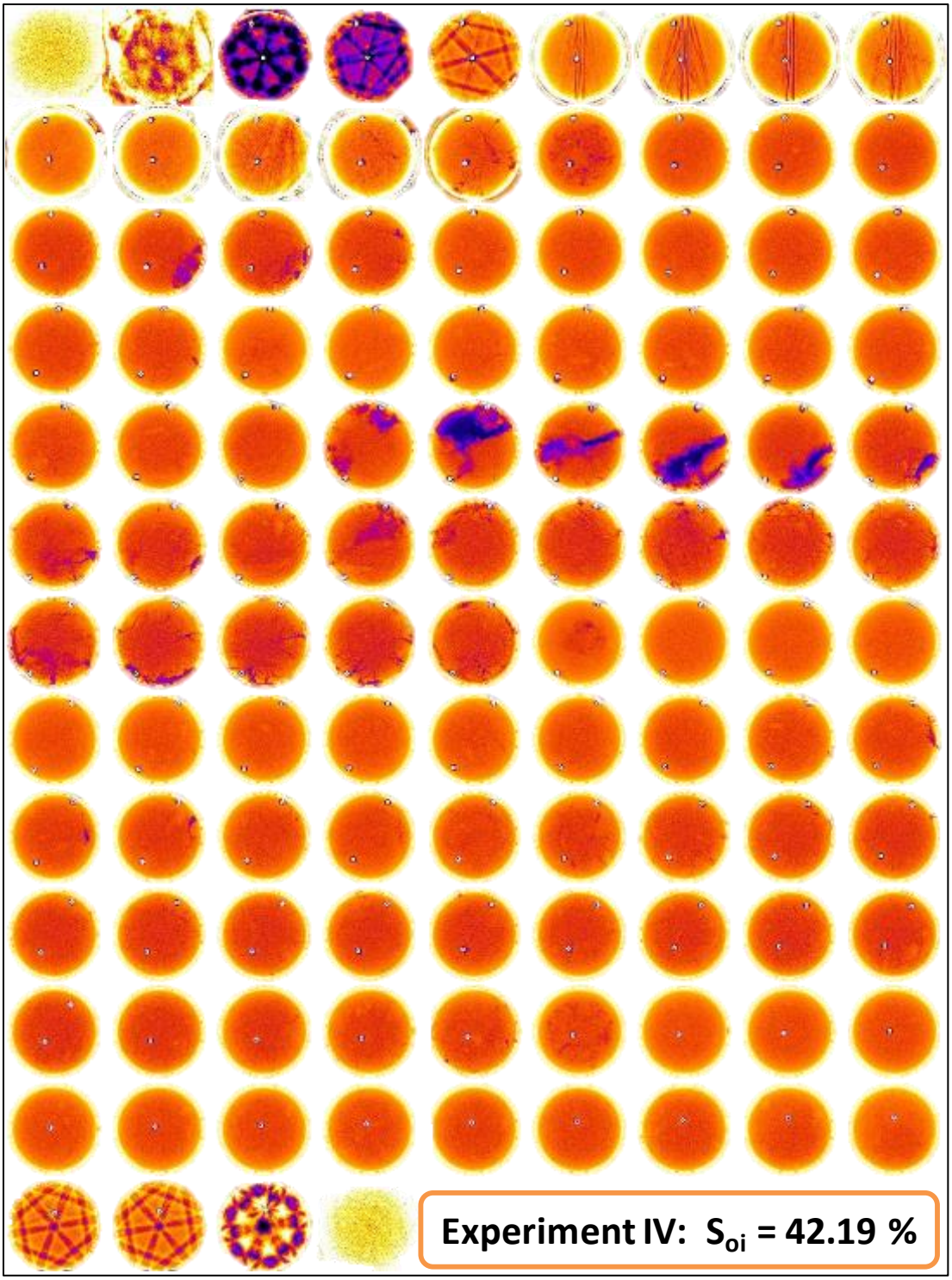

Figure 27. CT cross-sectional images taken after the Experiment IV (the image interval is 0.9 cm)

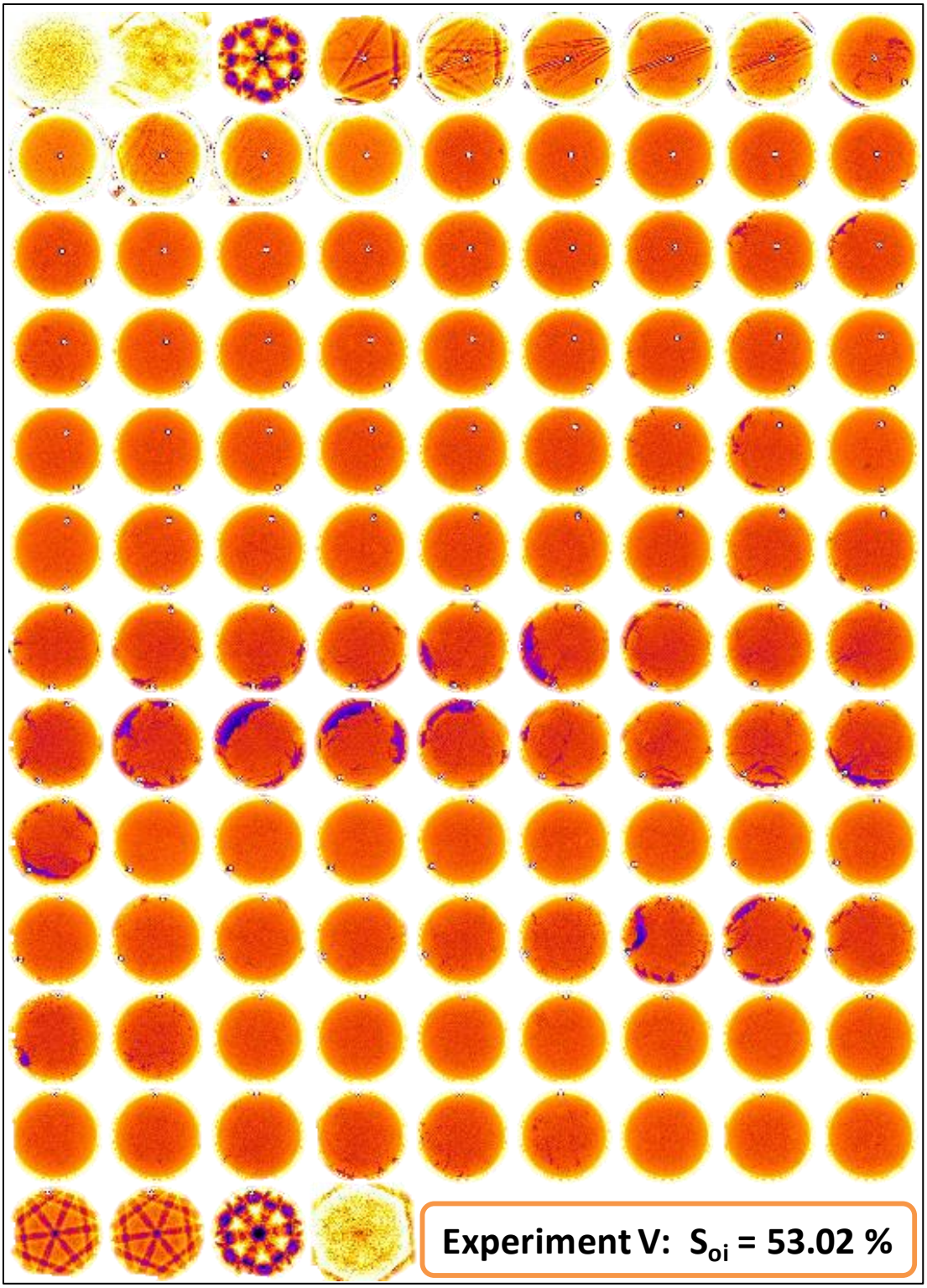

Figure 28. CT cross-sectional images taken after the Experiment V (the image interval is 0.9 cm)

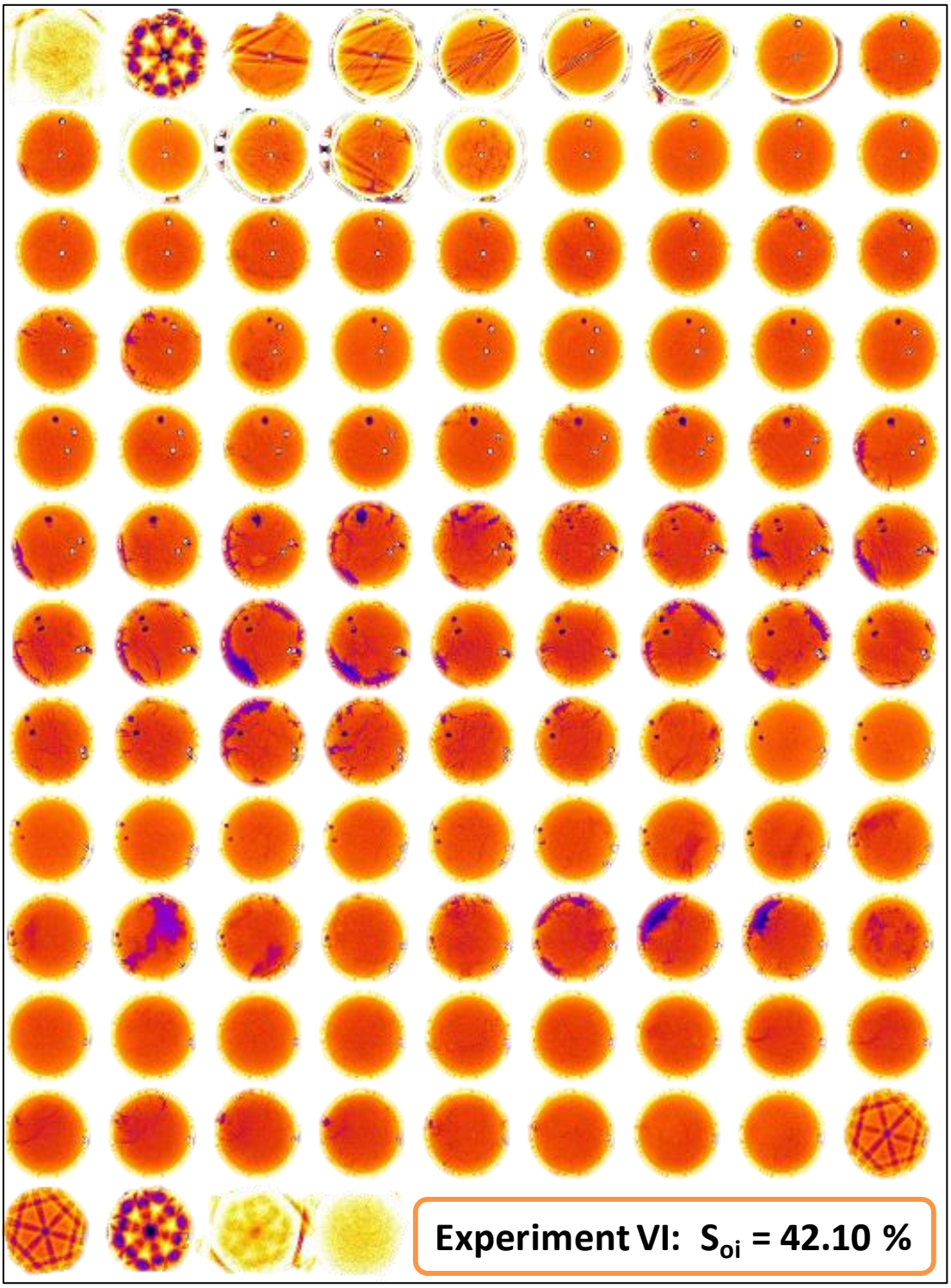

Figure 29. CT cross-sectional images taken after the Experiment VI (the image interval is 0.9 cm)